

Solvation Structures in Solid Polymer Electrolytes for Lithium-Based Batteries

Tao Chen,* Yuncong Liu, and Chao Wang*

Solid polymer electrolytes (SPEs) have gained widespread attention due to their potential applications in energy storage and conversion devices. The solvation structure, which refers to the interactions between polymers and ions in the electrolyte, plays a crucial role in the electrochemical performance of the electrolyte. This review summarizes the latest research progress in the solvation structures of SPEs, including their impact on ion conductivity, mechanical property, and interfacial stability. First, the characteristics of solvation structures in SPEs are introduced,

and they are compared with those in the liquid state. Then, some characterization techniques of solvation structures are listed, such as nuclear magnetic resonance (NMR), Raman spectroscopy, and X-ray diffraction. Subsequently, the influence of solvation structure on the performance of SPEs is analyzed, and the strategies for optimizing solvation structures through molecular design are discussed. Finally, future research directions are proposed aimed at developing high-performance SPEs by gaining a deeper understanding of solvation structures to meet the growing demands.

1. Introduction

The application of high-performance solid-state polymer electrolytes (SPEs) in lithium-based batteries offers significant advantages. With the growing demand for higher energy densities, enhanced safety, and long-term reliability, solid-state electrolytes are increasingly recognized as a viable replacement for traditional liquid-based electrolyte systems in energy storage applications, representing a key enabler in the advancement of lithium battery technology.^[1] SPEs not only mitigate safety risks by preventing liquid electrolyte (LE) leakage and thermal runaway but also improve the mechanical stability and temperature adaptability of batteries,^[2] thereby extending the range of applications for lithium-based energy storage systems. Consequently, in-depth studies on the chemical composition, structural design, and interface engineering of SPEs are crucial, not only for advancing lithium battery technologies toward higher performance goals but also for achieving sustainable energy storage, facilitating the widespread adoption of electric transportation, and promoting green energy systems.

Despite their immense potential, SPEs still face several critical challenges that hinder their widespread application. Firstly, the packing and crystallization of polymer molecules require a significant thermodynamic driving force, leading to relatively low

room-temperature ionic conductivity for conventional SPEs (10^{-8} to 10^{-6} S cm $^{-1}$).^[3] Secondly, in lithium batteries using metallic lithium as the anode, the complex electrochemical environment and the large volume changes associated with lithium dissolution and deposition can cause irreversible fracture or decomposition of the SPE during cycling, particularly under high-temperature conditions where mechanical stability is compromised.^[4] Furthermore, the interface stability between the SPEs and electrode materials remains a challenge, especially under high-voltage (>4 V) conditions, where SPEs with a narrow electrochemical window (e.g., polyethylene oxide (PEO)) are prone to oxidative degradation, leading to increased interfacial impedance and negatively impacting battery cycle life and charge-discharge efficiency.^[5] Therefore, improving the ionic conductivity, enhancing mechanical properties, and optimizing the interfacial compatibility of SPEs remain key issues to be addressed in SPEs research.

In recent years, extensive research has been conducted to enhance the performance of SPEs through blending,^[6] copolymerization,^[7] crosslinking,^[8] branching,^[9] grafting,^[10] and the use of additives.^[11] However, a comprehensive understanding of the underlying mechanisms driving these performance improvements and their insights remains incomplete. In this perspective, we explore the electrochemical behavior of lithium-based batteries from the viewpoint of the solvation structure of SPEs. We first elucidate the characteristics and driving forces behind the solvation structure of the electrolyte. Subsequently, we provide a detailed comparison of the solvation structures in SPEs and LEs and the resultant effects. Additionally, we describe the methods for characterizing the solvation structures within SPEs. Finally, we summarize the correlation between the solvation structure of SPEs and the observed electrochemical performance, incorporating strategies to optimize battery performance by adjusting the solvation structure. We believe this review offers a novel perspective that combines theoretical and experimental approaches, leveraging solvation design in

T. Chen
National Rail Transit Electrification and Automation Engineering
Technology Research Center
Southwest Jiaotong University
Chengdu 611756, P. R. China
E-mail: taochen12@swjtu.edu.cn

Y. Liu, C. Wang
Key Lab of Organic Optoelectronics & Molecular Engineering
Department of Chemistry
Tsinghua University
Beijing 100084, P. R. China
E-mail: chaowangthu@mail.tsinghua.edu.cn

SPEs to enhance the electrochemical performance of lithium-based batteries.

2. Electrolyte Solvation Structures in Lithium-Based Batteries

2.1. Interactions in Solvation Structures

Solvation refers to the process in which solutes are uniformly dispersed in a solvent and surrounded by solvent molecules. In SPE, the solvent is substituted with a polymer matrix. Various interactions will be formed during the solvation process. Ion-dipole interaction between lithium ion and polymer dipole is one of the key driving forces in the formation of solvation structure.^[12] Li⁺ ion have empty 2s orbitals after losing the outer electron, while dipoles are electron donors and can provide lone pairs of electrons. Dipoles with higher Lewis basicity have a higher electron-donating ability, so they can form stronger ion-dipole interactions with lithium ions. Furthermore, the structure of anions can also affect the ion-dipole interaction. Large anions with delocalized electrons will weaken the Coulombic interaction between anions and cations, resulting in a strong ion-dipole interaction.^[13]

Hydrogen bond (H-bond) is another interaction that exists in solvation structures. It forms between hydrogen and a more electronegative atom or group. Some fluorinated anions may form H-bond with hydrogen atoms on the polymer chain, inducing specific solvation structures and influencing the mobility of anions.^[14] Van der Waals forces also exist in solvation structures. They result from the basic electrical forces between positive and negative charges. These interactions are relatively weak, so they have been rarely mentioned in solvation structures in SPEs. However, a recent study in liquid LEs found that the molar quantity of solvent is always 10–12 times higher than that of cations and anions.^[15] The total strength of this weak interaction is sufficient to affect the performance of the electrolyte. More efforts have to be paid to study their influence in SPEs.



Tao Chen received his Ph.D. degree from the University of Chinese Academy of Sciences, China, in 2019. After that, he worked at the Department of Chemistry, Tsinghua University, as a postdoctoral fellow from 2019 to 2022. Now, he joins in the Southwest Jiaotong University. His main research interests focus on the solid polymer electrolytes design and interfacial regulation for lithium metal batteries.



Yuncong Liu obtained his bachelor's degree in Polymer Science and Engineering from South China University of Technology, China, in 2019, and is currently a Ph.D. candidate at the Department of Chemistry in Tsinghua University, China, under the supervision of Dr. Chao Wang. His research focus is on the design of ion-dipole interactions in polymers and their applications.

2.2. Solvation Structures in LEs vs. SPEs

2.2.1. Solvation Medium

In LEs, the solvation of lithium ions occurs through dynamic interactions with low-molecular-weight organic solvents, such as ethylene carbonate (EC) or dimethyl carbonate (DMC).^[16] The solvent molecules continuously exchange and adjust around the lithium ion, forming a fluid and flexible solvation shell.^[17] In contrast, in SPEs, the solvation of lithium ions is primarily achieved through coordination with polar functional groups within the polymer matrix, such as ether (—O—) or carbonyl (C=O) groups.^[18] These groups, embedded within the polymer chains, form a rigid, relatively static solvation shell around the lithium ion (Figure 1a). The polymer matrix serves as both the medium for solvation and the ion transport channel. The structure and stability of the solvation shell highly depend on the chemical composition of the polymer, the flexibility of its segments, and the dispersion of the lithium salt.

2.2.2. Solvation Shell Composition

In LEs, lithium ions are surrounded by a solvation shell formed by 2 to 6 solvent molecules, depending on the solvent's polarity and its ability to coordinate with the lithium ion.^[19] This solvation shell is highly dynamic, with continuous exchange of solvent molecules and a more flexible, less constrained environment (Figure 1b).^[20] In contrast, the solvation shell in SPEs is composed of several polar functional groups that provide a stable yet rigid solvation environment.^[21] These interactions typically involve coordination of one or a few polymeric functional groups to the lithium ion. The solvation shell is relatively fixed due to the constraints imposed by the polymer chain structure (Figure 1c).

The dielectric constant of polymers is much lower than that of small molecules, and they can be considered as weak electrolyte systems.^[22] To generate mobile ions in polymers, it is necessary to introduce a high concentration of polar groups into the polymers, constructing strong ion-dipole interactions. The lower dielectric constant also leads to the frequent presence of contact ion



Chao Wang earned his Ph.D. degree from Tsinghua University, China, in 2011. After that, he conducted his postdoctoral research at Stanford University. Since 2018, he has been assigned as an associate professor in the Department of Chemistry, Tsinghua University. His current research interests focus on the new energy materials, ionic conductors, and stretchable electronics.

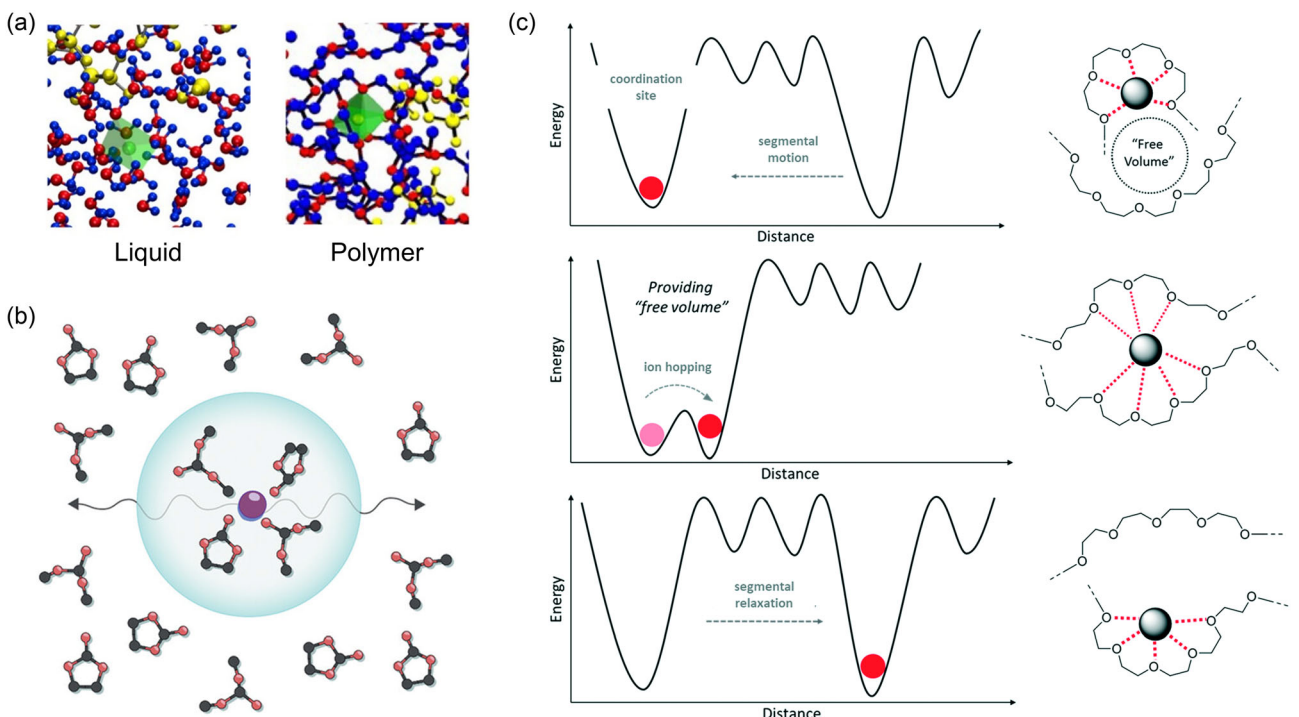


Figure 1. a) Solvation structures of lithium ions in liquid and solid electrolytes (reprinted with permission.^[26] Copyright 2021, Elsevier Inc.). b) Mobile ion-solvent complexes in LEs (reprinted with permission.^[30] Copyright 2023, The Authors). c) Theoretical representation of ionic conduction pathways in PEO-type polymer electrolytes based on the free volume model (reprinted with permission.^[32c] Copyright 2019, The Royal Society of Chemistry).

pairs (CIP) and multi-ion aggregates (AGG) structures in polymers, which means anions will enter the inner solvation sheath.^[23] This special solvation structure can also affect the electrical properties of the material.

2.2.3. Dynamicity and Ion Transport

In LEs, the solvation shell is highly dynamic, allowing for rapid solvation and desolvation of lithium ions.^[24] This results in a much higher ionic conductivity, generally in the range of 10^{-2} to $10^{-3} \text{ S cm}^{-1}$, due to the free movement of solvent molecules and the efficient ion transport enabled by the solvation-exchange process.^[25] The high dynamicity of the LE solvation shell contributes to its superior ionic conductivity, though it also introduces potential challenges related to interfacial stability and safety, particularly at elevated temperatures.

In contrast, a key distinction in SPEs lies in the rigidity of their solvation structures, which is largely dictated by the polymer's glass transition temperature (T_g) and the mobility of its chain segments.^[26] The ion transport mechanism in SPEs is governed by a "creeping" process, where lithium ions move along the polymer chains via local segmental motion.^[27] This results in relatively low ion conductivity, typically below $10^{-4} \text{ S cm}^{-1}$ at room temperature, as the ion transport is limited by the mobility of the polymer chains.^[28]

2.2.4. Ion Transport Mechanism

In traditional dilute electrolytes, ions are capable of migrating either autonomously or in conjunction with their surrounding

solvent molecules, which is known as vehicular transport. In high-concentration electrolytes (HCEs), ions may move independently by continuously exchanging their neighboring solvent particles through a structural diffusion mechanism.^[29] Consequently, the timescale related with these alterations in the solvation environment is a critical component of the ion transport process.^[30]

Unlike LEs, SPEs comprise more complicated structures, including both amorphous and crystalline fractions at room temperature. The forms of ion conduction vary among different structures. Here, we take PEO as an example. Ion transport principally occurs in the amorphous regions in three ways based on how ions move with the polymer chains: (i) ion motion along the polymer chain (intrachain), (ii) intersegmental ion hopping between ion solvation sites, and (iii) ion polymer codiffusion.^[31] The intrachain ion motion is a process of continuous ion diffusion, where an ion switches from one neighboring monomer to another. If the new monomer comes from a nearby polymer chain, we call this a continuous chain exchange. The ion hopping between different parts of the polymer can happen within one chain or between different chains.^[32] This often involves changing several monomer units that are all connected to the same ion at the same time. The transport mechanism in the amorphous region is consistent with the structural mechanism. The time an ion stays in one place before hopping to another (the hopping time, τ_{hop}) depends on how the ion's solvent sites are connected.

In contrast, ion transport is hindered in crystalline phases because the polymer segments are immobilized, such as in the helical conformation of PEO within the crystalline structure of $(\text{PEO})_3\text{LiCF}_3\text{SO}_3$.^[33] However, for well-defined crystalline

complexes (e.g., $(\text{PEO})_6$ lithium hexafluoroarsenate), ion transport can occur through the hopping of lithium ions between adjacent sites.^[34] It is important to note that the molecular weight of PEO and the type of lithium salt are critical factors for ensuring rapid ion transport, as the ion hopping pathways are strongly dependent on the availability of defects within these crystalline polymers.

The solvation structure in SPEs is central to the transport behavior of lithium ions. Although their dynamics are weaker than those of LEs, their higher interfacial stability and safety make them an important candidate for the next generation of high-energy-density batteries. In the future, optimizing the solvation structure of SPEs (such as by introducing functionalized polymers or designing nanocomposites) will become an important strategy to enhance their conductivity, appropriate mechanical properties, and interfacial stability.

3. Characterization of Solvation Structure in SPEs

The solvation structure in SPE greatly affects the electrolyte performance. The precise characterization and description of the interaction of ions and molecules is crucial to understand the solvation structures. Spectroscopic techniques can provide valuable information by analyzing changes in bond vibration, rotation, and atom electron cloud density. These techniques reveal solvation processes at the molecular level and help us to understand the behavior of ions in solvation structures. With the development of computational chemistry, computational methods, such as molecular dynamics (MD) simulations, have become a new tool for visualizing the solvation structures. It can simulate and predict the microscopic dynamic behavior of ions and molecules in electrolytes. The combination of these methods allows us to deeply understand the solvation structures in SPEs from multiple perspectives.

3.1. Spectroscopic Techniques

Raman spectroscopy is a molecular spectroscopy. It works on the principle of Raman scattering, which produces scattered photons with a different frequency depending on the vibrational and rotational properties of the scattered molecules.^[35] It has been widely used in the characterization of solvation structures in SPEs.^[36] Edman et al. utilized Raman spectroscopy to study the ion pair formation in $\text{P}(\text{EO})_n\text{LiTFSI}$ system as a function of composition, temperature, and physical state.^[37] The 740 cm^{-1} mode of the bis(trifluoromethanesulphonyl)imide (TFSI) anion was used as a probe of ionic interactions. The Raman spectra in the $728\text{--}752\text{ cm}^{-1}$ shows the majority of anion species is free TFSI in the crystalline phase for $n \geq 6$. When PEO became amorphous at high temperature ($T = 70^\circ\text{C}$), the amount of ion pairs was still small for $n \geq 8$ but significant in the salt-rich $\text{P}(\text{EO})_6\text{LiTFSI}$ sample. Another band at 863 cm^{-1} is related with polymer segments involved in Li^+ solvation. In all-amorphous $\text{P}(\text{EO})_n\text{LiTFSI}$ electrolytes with high salt concentration ($n = 6$), the decreased intensity of the band indicates less ether oxygens participate in the

solvation. It results in the increment of contact ion pair formation and lithium cations are solvated by a combination of ether oxygens and TFSI anions.

A notable technical limitation in Raman spectroscopy arises from sample fluorescence induced by NIR/visible laser excitation. The fluorescence background, being substantially more intense than Raman signals, can effectively mask the characteristic Raman scattering peaks, compromising spectral quality and analytical accuracy. We can use the ultraviolet light excitation method to reduce the influence of fluorescence.

FTIR spectroscopy, similar to Raman spectroscopy, studies molecular vibrations but uses a different approach. While Raman looks at how light scatters and how molecules' electron clouds change shape, FTIR measures how much infrared light gets absorbed when molecules' electrical asymmetry changes. Because FTIR works by absorption, its signals are usually stronger and easier to measure quantitatively using different mathematical analysis methods. The research team led by Tominaga utilized FTIR spectroscopy to analyze how solvation structures influence ionic conduction in poly(ethylene carbonate) (PEC)-based electrolytes containing lithium bis(fluorosulfonyl)imide (LiFSI).^[38] The peak around 1740 cm^{-1} in FTIR is ascribed to $\text{C}=\text{O}$ stretching vibration. After the addition of lithium salt, a new peak at 1720 cm^{-1} is appeared due to the formation of $\text{C}=\text{O}\cdots\text{Li}^+$ interaction. The peak corresponding to free $\text{C}=\text{O}$ gradually becomes smaller with increasing concentration of LiFSI. The proportion of $\text{C}=\text{O}\cdots\text{Li}^+$ is nearly saturated above 50 mol%. The Raman spectra show all the FSI anions exist as AGGs when the concentration exceeds 50 mol%. The highly aggregated ionic structure allows the electrolytes to have high t_+ .

Solid-state nuclear magnetic resonance (ssNMR) spectroscopy serves as a powerful analytical technique for elucidating atomic-scale structural and dynamic properties of solid materials. This method's distinctive capability lies in its sensitivity to subtle variations in magnetic environments, enabling the differentiation of chemically equivalent atoms based on their local structural contexts.^[39] Natural abundant light elements, such as ^1H , ^6Li , ^7Li , ^{13}C , ^{17}O , and ^{19}F , are normal nucleus used to study the solvation structure.^[40] Chen's group created a solid polymer electrolyte (SPE) by using UV light to combine three ingredients: a conducting pyrrole-based ionic liquid, vinyl ethylene carbonate (VEC) molecules, and a fluorine-containing linking agent (OFHDODA).^[41] They found the ionic conductivity of the SPE increased from 0.49 to 1.37 mS cm^{-1} when the content of VEC increased from 8.7 to 22.2 mol%. They used ^6Li ssNMR to explore the effect of VEC contents on the Li^+ transport energy barrier. The ^6Li ssNMR spectrum of $\text{P}(\text{IL-OFHDODA-VEC})$ exhibits three distinct chemical shifts at -0.2 , -1.7 , and -2.9 ppm . The predominant peak at -0.2 ppm , accounting for $\approx 55\%$ of the total signal intensity, signifies a substantial transition of lithium ions from strongly coordinated states to weaker binding environments. This spectroscopic evidence suggests that VEC integration enhances LiTFSI dissociation within the polymer matrix, thereby facilitating improved ionic conductivity at ambient temperature (25°C).

While the aforementioned analytical techniques demonstrate excellent sensitivity for characterizing local molecular interactions and orientations at sub-nanometer scales ($<1\text{ nm}$), they

exhibit significant limitations in probing structural features at intermediate (1–10 nm) and extended (>10 nm) length scales, presenting a notable gap in comprehensive material characterization.^[42] Small-angle scattering (SAS) represents a powerful analytical method for investigating structural organization across multiple length scales, spanning from the ångstrom range to the micrometer regime.^[43] Small-angle X-ray scattering (SAXS) and small-angle neutron scattering (SANS) are two widely used SAS techniques to explore solvation structures in SPEs. Through SAXS analysis, Balsara and colleagues investigated the correlation between morphological characteristics and ionic transport properties in single-ion-conducting diblock copolymers composed of poly(ethylene oxide) and polystyrenesulfonyllithium(trifluoromethylsulfonyl)imide (PEO-PSLiTFSI) domains.^[44] During thermal treatment, SAXS measurements were conducted to obtain the scattering intensity (I) as a function of the scattering vector (q) for the PEO-PSLiTFSI copolymer (Figure 2a). At room temperature, the SAXS peak at $q = q_c = 1.33 \text{ nm}^{-1}$ correlates with the ion cluster in PEO-PSLiTFSI. The scattering peak at $q = q^* = 0.228 \text{ nm}^{-1}$ indicates the presence of a lamellar morphology. The characteristic intercluster spacing, denoted as d_{cluster} , was determined to be $\approx 4.7 \text{ nm}$ ($d_{\text{cluster}} = 2\pi/q_c$). The intensity of the peaks decreases substantially above 50 °C, but the changes of intensity are reversible when the sample is cooled. The research findings demonstrate that lithium ions remain confined within ionic clusters in the low-temperature lamellar phase. Upon reaching a critical transition temperature, the system undergoes a thermodynamic phase change to a disordered state, facilitating ion dissociation from clusters and resulting in a dramatic enhancement of ionic conductivity by multiple orders of magnitude (Figure 2b).

Neutron-based characterization techniques offer distinct advantages over X-ray methods, particularly in terms of penetration depth due to their neutral charge. Furthermore, the nuclear scattering mechanism of neutron-matter interactions provides enhanced sensitivity to lithium species, a capability that X-ray techniques typically lack.^[45] SANS employs elastic neutron scattering phenomena within the low wavevector regime ($10^{-3} \text{ nm}^{-1} < Q < 10^{-1} \text{ nm}^{-1}$) to investigate nanoscale structures. This technique provides exceptional capability for characterizing the spatial organization and temporal evolution of dispersed aggregates within continuous matrices. The research team led by Balsara employed SANS techniques to quantitatively assess how LiTFSI salt incorporation affects the molecular dimensions and chain conformation of PEO in electrolyte mixtures.^[46] Analysis of the Kratky plots derived from scattering profiles reveals an inverse correlation between salt concentration and polymer segment length at lower salt concentrations. At high salt concentrations, it increases with increasing salt concentration (Figure 2c). The scattering data from deuterated PEO-LiTFSI systems indicates the presence of well-defined ion clusters measuring $\approx 0.6 \text{ nm}$ in size, which become prominent at higher salt loading levels (Figure 2d).

Quasielastic neutron scattering (QENS) represents a sophisticated neutron spectroscopy technique capable of probing MD across temporal (picosecond to nanosecond) and spatial (ångstrom to nanometer) domains. This method relies on precise measurement of minute energy exchanges (typically within $\pm 2 \text{ meV}$) between incident and scattered neutrons during scattering events.^[47] This technique enables comprehensive characterization of MD spanning multiple timescales, from rapid vibrational

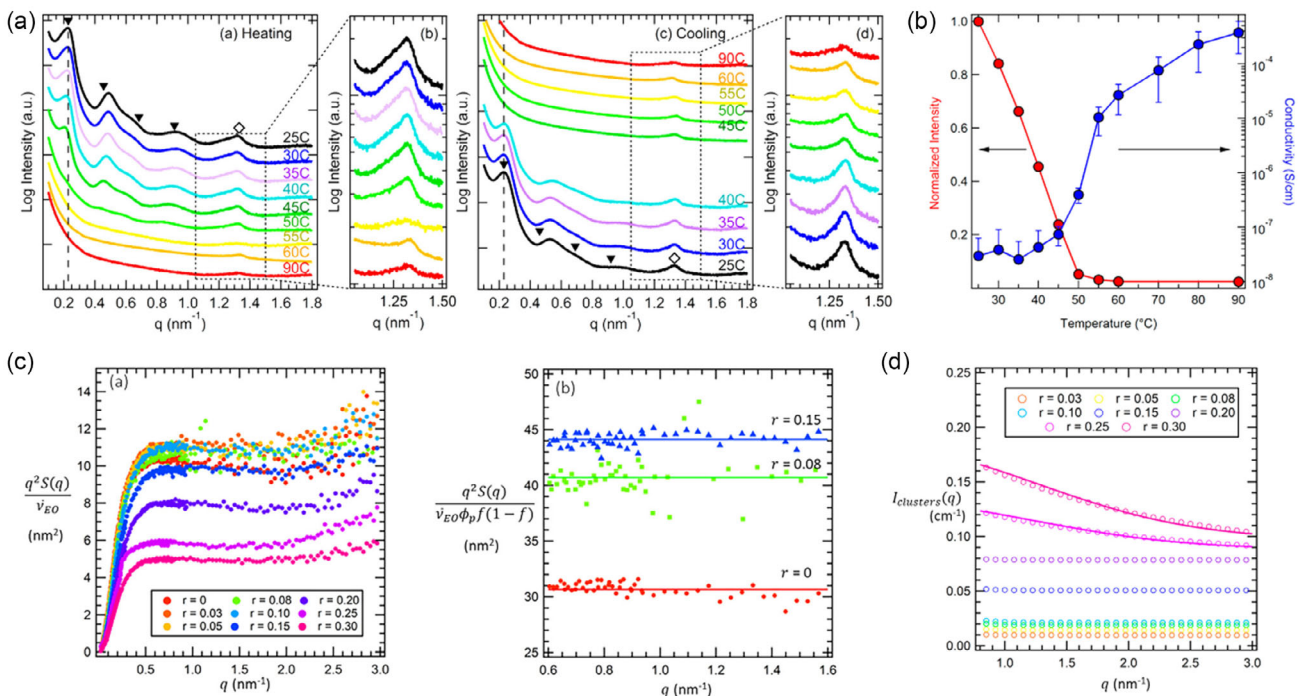


Figure 2. a) Temperature-dependent SAXS profiles for the PEO-PSLiTFSI electrolyte. b) Conductivity and SAXS results of the PEO-PSLiTFSI electrolyte (reprinted with permission.^[44] Copyright 2014, American Chemical Society). c) Kratky plots and normalized Kratky plots $q (\text{nm}^{-1})$ for the blends at varying salt concentrations. d) Scattering profiles of ion clusters in pure dPEO/LiTFSI mixtures at elevated salt concentrations (reprinted with permission.^[46] Copyright 2019, American Chemical Society).

modes to slower diffusive processes. Saboungi et al. studied the relaxation of pure PEO and PEO electrolyte on a nanosecond timescale using QENS.^[48] The difference in scattering characteristics between pure PEO and PEO electrolyte can be attributed to the addition of lithium salt which causes the dynamic alterations in the polymer chains. The analysis revealed that the polymer electrolyte's dynamics are governed by multiple distinct processes: (1) a slow translational mode and (2) one or two rapid rotational modes originating from conformational fluctuations of chain segments between crosslinking points. Balsara and Wang et al. used QENS to measure the solvation dynamics in poly(pentyl malonate) (PPM)-LiTFSI polymer electrolyte.^[49] Analysis of the time-dependent segmental motion revealed excellent agreement with the Rouse model predictions for salt-free polymer systems, as evidenced by the characteristic mean-squared displacement behavior. The experimental data reveals a characteristic reduction in the Rouse parameter followed by stabilization as salt concentration increases. This behavior indicates the formation of transient crosslinks mediated by lithium ion coordination with multiple polymer chains. Quantitative analysis shows these dynamic crosslinks persist for ≈ 1 ns in the PPM/LiTFSI system, reflecting the slow kinetics associated with solvation shell reorganization in polymer electrolytes.

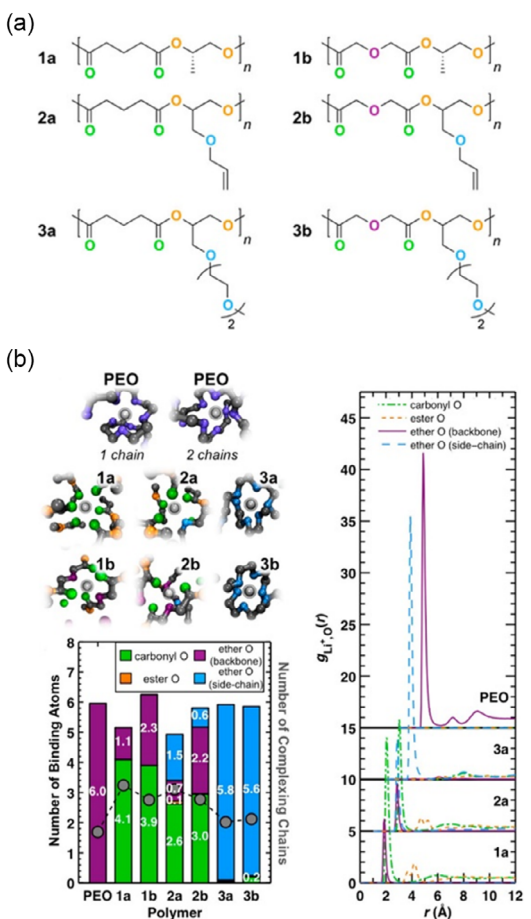


Figure 3. a) Repeat units for polyesters. b) Analysis of lithium-ion coordination data obtained from MD simulations conducted at 363 K (reprinted with permission.^[53] Copyright 2015, American Chemical Society). c) Representative snapshots of LiTFSI coordination and corresponding density-weighted lithium-oxygen RDFs (atoms per nm³) in PTHF and PEO (reprinted with permission.^[54] Copyright 2018, Wiley-VCH GmbH).

3.2. Theoretical Simulation

Theoretical models at the macro- and microscales for SPEs aim to describe the solvation environment of ions. MD simulation represents a powerful computational technique that models the temporal evolution of atomic and molecular systems through numerical integration of Newtonian equations of motion, providing detailed insights into system dynamics at the molecular level.^[50] In the study of the solvated structure of electrolytes, the systems involved in the simulation include electrolyte ions and solvent molecules. Through simulations, we can observe how ions and solvent molecules interact in space and time to form specific solvated structures.^[51]

An initial model system needs to be built before conducting MD simulations. Then, the interaction between the ion and the molecule is described by defining an appropriate potential energy function. These potential energy functions can be empirical or calculated based on quantum mechanics. Next, numerical methods are used to solve Newton's equations of motion to simulate the evolution of the system over time. Choosing the right potential energy function is the key to accurate simulation. For the interaction between ions and solvent molecules, electrostatic forces, hydrogen bonds, and van der Waals forces usually need to be considered. The parameters of these interactions can be

obtained through experimental data or quantum chemical calculations. During the simulation, the solvated shell can be determined by analyzing the distribution of solvent molecules around the ions. This involves calculating the radial distribution function (RDF) between the ion and the solvent molecule. RDF can provide information about the size and structure of the solvated shell, such as the thickness of the first solvated shell and the arrangement of solvent molecules.^[52] One advantage of MD simulation is the ability to study the dynamic characteristics of solvated structures. Through simulations, we can observe the changes in the solvated shell over time, including the exchange of solvent molecules and the migration of ions. This dynamic information is important for understanding the conductivity and diffusion properties of electrolyte solutions.

Miller et al. taken long-timescale MD simulations to investigate lithium-ion solvation and diffusion in six polyester SPEs.^[53] They found that among the studied polymers, PEO exhibits unique coordination behavior, frequently forming single-chain lithium cation complexes and demonstrating substantial intrachain lithium ion mobility through hopping mechanisms. For type-1 polymers (Figure 3a), the lithium ion preferentially coordinated with carbonyl oxygens on the polymer backbone, and the side chain has no affinity for the lithium ion. In type-2 and type-3 polymeric systems, oxygen moieties within side chain structures demonstrate significant lithium ion coordination capability. Notably, type-3 polymers exhibit exclusive lithium ion complexation through their PEO-analogous side chains (Figure 3b).

Bao et al. used MD simulation to study the Li⁺ coordination environment in poly(tetrahydrofuran) (PTHF).^[54] The representative snapshots demonstrate that the extent of anion separation is significantly greater for LiTFSI in PEO compared to that in PTHF (Figure 3c). Furthermore, the PEO backbone is observed to adopt the well-known “helical” conformation, effectively wrapping around the Li⁺ ion. PTHF forms a more disordered solvation shell around lithium. The Li⁺-O RDFs reveal that, on average, ≈6 oxygen atoms solvate each Li⁺ ion in the PEO system, whereas only about 4 oxygen atoms are involved in solvating Li⁺ in PTHF. These findings indicate that PTHF exhibits weaker coordination to lithium compared to PEO.

4. Correlation between Solvation Structures and Properties in SPEs

4.1. Ion Transportation

The solvation structure within SPEs is critically important, as it significantly influences the migration dynamics of Li⁺ ions and plays a key role in modulating ion transport.^[38,55] The solvation process determines the interaction between Li⁺ and the polymer chains, both intra- and interchain, thereby influencing its migration pathways and rates within the SPEs.^[56] Wang et al.^[49,57] through MD simulations and wide-angle X-ray scattering (WAXS) experiments, found that in polymer electrolytes composed of PEO and lithium salts, the polymer tends to coordinate with Li⁺ via single chains. This strong and tight solvation structure results in a high

desolvation energy barrier for Li⁺ in PEO-based solid-state electrolytes, which limits the Li⁺ transference number and restricts the fast charge/discharge capability. In contrast, in electrolytes with poly(pentamethylene adipate) (PPM) as the polymer, Li⁺ coordinates with oxygen atoms from 2 to 3 surrounding chains as well as an anion, forming a looser solvation structure (Figure 4a). Meanwhile, the more polar polymer chains provide shielding effects for the anions, which results in a higher transference number for Li⁺ in PPM compared to PEO. In our view, for pure PEO-based polyether electrolytes, the solvation effect on Li⁺ is too strong and needs to be appropriately weakened. For polyester-based electrolytes, although the Li⁺ transference number is improved, the involvement of multiple chains in ion coordination, along with the stronger dipole–dipole interactions between the more polar polymers, may lead to a higher T_g , restricting the ion migration path and resulting in a lower ionic conductivity compared to PEO.

The solvation structure can optimize the freedom of Li⁺ by adjusting its solvation shell, reducing adhesion to the polymer matrix, and thus enhancing Li⁺ mobility.^[21] Excessive solvation might overly “trap” Li⁺ within the polymer matrix, leading to restricted ion transport, while insufficient solvation may hinder the solubility of lithium salts in the polymer matrix, resulting in lower dissociation between Li⁺ and anions and consequently limiting the concentration of ionic charge carriers, which also restricts ion transport.^[58] An appropriate degree of solvation, however, can promote the effective diffusion of Li⁺ within the electrolyte. Additionally, the flexibility of the polymer chains and their polarity significantly influence the solvation structure, further affecting the ionic conductivity of the electrolyte.^[58b]

By finely tuning the solvation structure, the Li⁺ transport properties of SPEs can be significantly enhanced, thereby enhancing the overall performance and stability of solid-state lithium batteries. Juan J. de Pablo et al.^[59] through simulation studies, explored the solvation structure and ion transport behavior of Li⁺ in poly(oligo ethylene methacrylate) (POEM) and its copolymers with poly(glycerol carbonate methacrylate) (PGCMA). Their study revealed that, despite the high polarity of PGCMA, Li⁺ preferentially coordinates with ether oxygens rather than with PGCMA due to the lower entropy penalty (Figure 4b). This finding challenges the conventional view that higher polarity solvents are more conducive to ion dissociation. The presence of PGCMA dilutes the concentration of ether oxygens, reducing interchain hopping and increasing single-chain solvation, which optimizes Li⁺ transport. This dilution effect is advantageous in the random copolymer PGCMA-r-POEM, where PGCMA and ether segments form mixed solvation sites that help establish a more continuous Li⁺ transport network. However, in the block copolymer PGCMA-b-POEM, PGCMA localizes in regions that are unfavorable for Li⁺ transport, which impedes the ion mobility. These findings provide insights into how thermodynamic driving forces control the solvation and transport of lithium ions in blended SPEs. Furthermore, Chen et al.^[60] optimized the solvation structure of Li⁺ in SPEs by precisely controlling polymer sequences. They demonstrated the use of alternating copolymer single-ion polymer electrolytes (Alter-SPEs), where the sequence

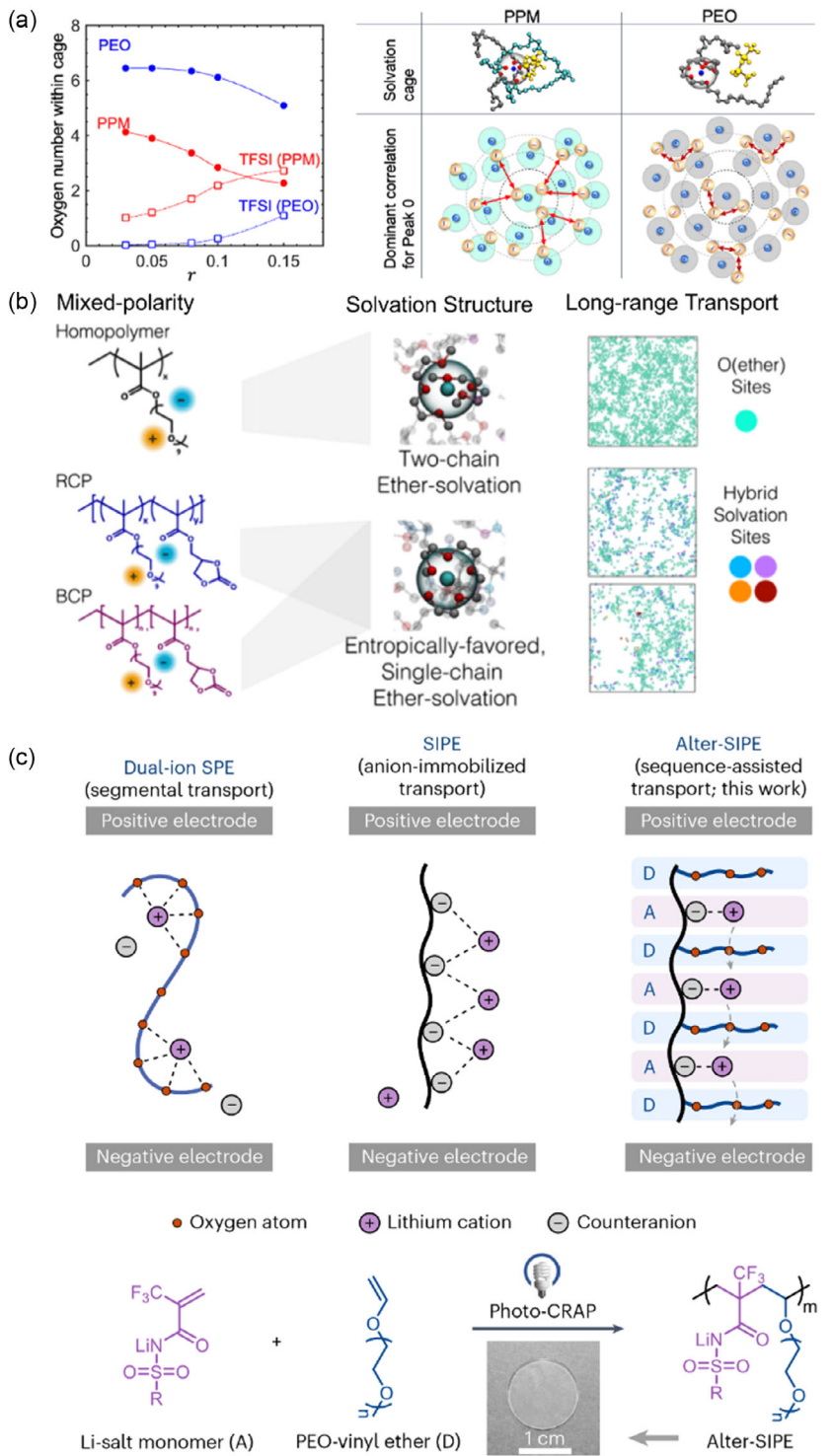


Figure 4. a) Simulation of solvation structure based on PEO and PPM (reprinted with permission.^[57] Copyright 2023, American Chemical Society). b) Simulation of solvation structure based on homopolymer POEM, random copolymer PGCMA-r-POEM, and block copolymer PGCMA-b-POEM (reprinted with permission.^[60] Copyright 2023, The Authors). c) Illustration of Li⁺ transport mechanisms during battery charging in various polymer electrolyte systems, along with the synthesis process of Alter-SIPE (reprinted with permission.^[61] Copyright 2023, Springer Nature).

arrangement of anions and PEO side chains promotes uniform distribution of Li⁺ ions and non-aggregated Li⁺-anion solvation, thereby enhancing Li⁺ dissociation and migration (Figure 4c). The Alter-SIPE P8, for example, exhibited a Li⁺ transference number of 0.93 at 30 °C, with an ionic conductivity of $4.2 \times 10^{-5} \text{ S cm}^{-1}$,

which is substantially higher than that observed in both random and block copolymer SIPEs.

The configuration and distribution of polymer chains in the polymer topology are closely related to the Li⁺ solvation structure in SPEs, significantly affecting their ionic conductivity.^[61] The high

chain flexibility of linear polymers helps form a dynamic solvation environment, providing a lower energy barrier for Li^+ migration. However, excessive flexibility may lead to interchain packing, restricting ion diffusion.^[21] In contrast, branched or crosslinked topologies increase the free volume of the polymer, creating additional pathways for ion migration.^[62] However, excessively high crosslinking densities may reduce the chain's flexibility, inhibiting ion transport.^[63] Moreover, hyperbranched polymers or crosslinked networks can form locally ordered solvation environments within the matrix, enhancing the directional solvation of Li^+ , thereby improving ion migration efficiency. Therefore, polymer topology can optimize the ionic conductivity of SPEs by controlling the dynamics and uniformity of the solvation shell,

as well as the migration pathways and energy barriers for ions. Wu et al.^[64] reported a hyperbranched structure polymer electrolyte based on poly(3-hydroxy-3-methyl-oxazolidine) (PHMP), prepared via ring-opening polymerization. MD simulations revealed seven optimized solvation structures, where one Li^+ ion coordinates with oxygen atoms on different branches via ion-dipole interactions, fundamentally altering the traditional PEO solvation structure, where a single Li^+ is solvated by a continuous chain of oxygen atoms. The binding energies of these ion-solvation structures range from -4.47 to -5.66 eV (Figure 5a), indicating a significant reduction in the interaction between PHMP and Li^+ . Furthermore, due to the lower T_g of PHMP, the segmental motion at room temperature is enhanced, facilitating efficient Li^+

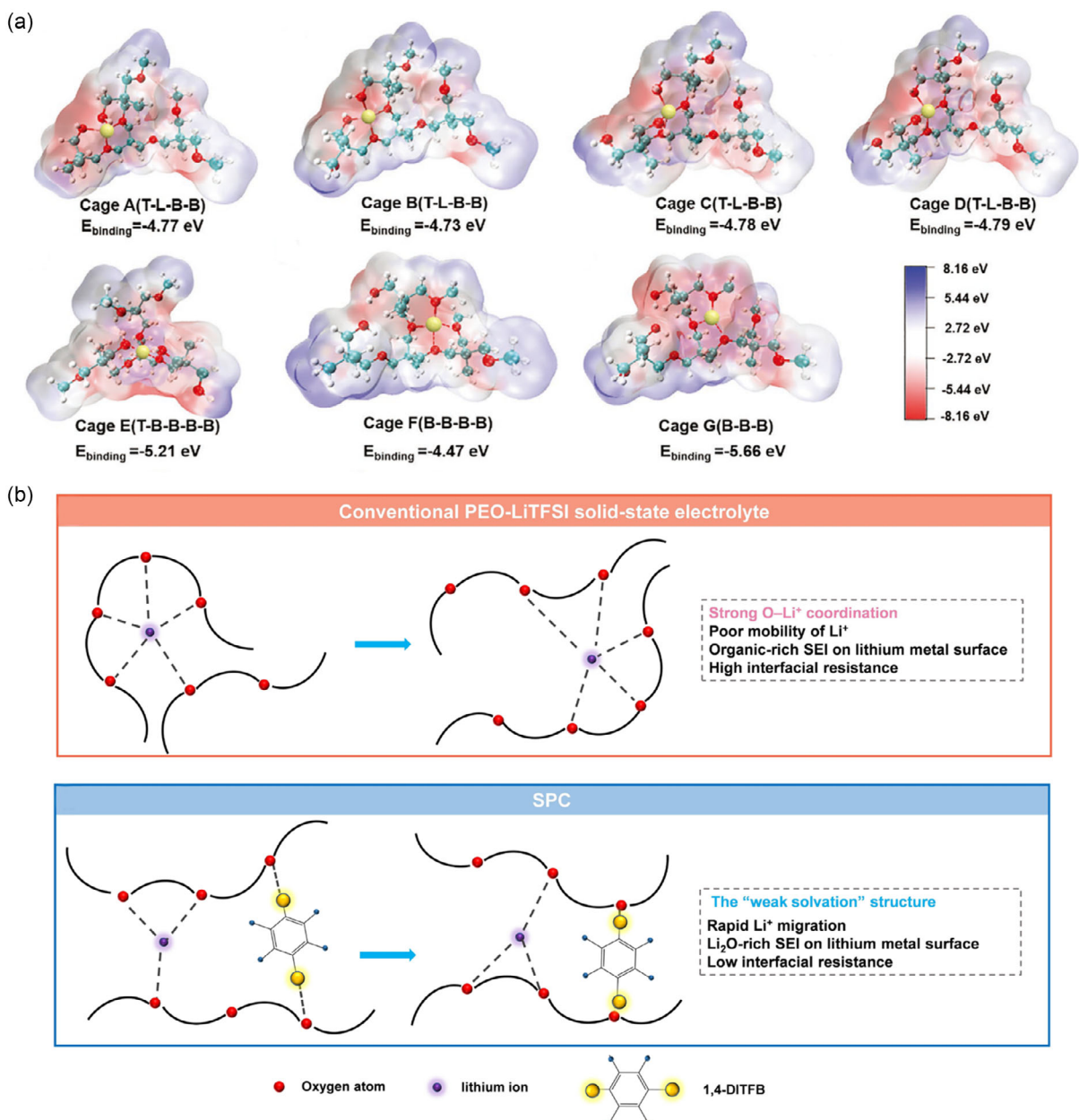


Figure 5. a) Different solvation structures and binding energies in PHMP electrolyte (reprinted with permission.^[65] Copyright 2021, Wiley-VCH GmbH). b) 1,4-DITFB as an additive regulated PEO-based electrolyte (reprinted with permission.^[69] Copyright 2023, Wiley-VCH GmbH).

diffusion. When 1.5 mol kg⁻¹ of LiTFSI is added, the ionic conductivity reaches 1.26×10^{-4} S cm⁻¹.

In addition to the molecular structure of the polymer matrix, the anions in SPEs also significantly impact both the solvation structure and ion transport properties. For instance, Peter G. Bruce et al.^[32c] showed that the AsF₆⁻ anion in the PEO₆:LiAsF₆ complex facilitates a solvation structure conducive to ion transport in crystalline regions, likely attributable to its weak coordinating ability. Cui et al.^[65] demonstrated that strengthening the interactions between anions and the polymer matrix effectively immobilizes anions, while the incorporation of high-dielectric-constant units promotes lithium salt dissociation. This synergistic effect enhances the concentration of free lithium ions and increases the lithium-ion transference number. Besides, different anions may induce distinct polymer conformations and crystallinity, thereby impacting ion mobility. The anion-mediated modulation may also reduce the effective binding energy between Li⁺ and the polymer, enhancing ion mobility by favoring transient coordination states over persistent ion pairing. Therefore, by judiciously selecting anions with appropriate size, polarizability, and electronic characteristics, it is possible to tailor the solvation landscape across various polymer electrolytes.^[66] This approach offers a promising pathway to optimize ionic conductivity and overall battery performance.

Moreover, the incorporation of additives in SPEs can further regulate the solvation structure through intermolecular interactions, thereby improving the ionic conductivity of the electrolyte.^[67] Specifically, additives can optimize the Li⁺ solvation shell by interacting with lithium salts or polymer chains, reducing the binding energy between Li⁺ and coordination groups, and enhancing their mobility. Additives can further enhance the segmental motion of the polymer matrix, thereby improving the continuity and efficiency of ion conduction pathways. Liu et al.^[68] introduced 1,4-diiodotetrafluorobenzene (1,4-DITFB) into a PEO-based electrolyte to modify the solvation structure of Li⁺. The electron-deficient iodine atoms in 1,4-DITFB can form halogen bonding with the electron-rich oxygen atoms in PEO, weakening the coordination between Li⁺ and oxygen (Figure 5b). MD simulations revealed that in the electrolyte without 1,4-DITFB, one Li⁺ ion coordinates with an average of five oxygen atoms. After adding 1,4-DITFB, the coordination number decreased to 4.6, and the Lennard-Jones potential shifted from -801.3 kcal mol⁻¹ to -781.2 kcal mol⁻¹, indicating that the constructed weak solvation structure effectively lowered the migration energy barrier for Li⁺, thereby improving migration kinetics. The resulting polymer electrolyte exhibited a room temperature conductivity of 1.2×10^{-4} S cm⁻¹ and a Li⁺ transference number of 0.35 ± 0.04 , which is significantly higher than that of traditional PEO-based electrolytes. Besides, Huang et al.^[69] introduced a very low content (less than 0.5 wt%) of CuF₂ as a Lewis acid additive into a PEO electrolyte. Through intermolecular Lewis acid-base interactions, the copper-coordinated polymer exhibited rich coordination chemistry, leading to a customized molecular structure. Specifically, the coordination interaction between Cu²⁺ and oxygen atoms in the PEO/LiTFSI material enhanced the ionic

conductivity. As a result of the weakened interaction between Li⁺ and the ether oxygen in PEO, TFSI⁻ was also fixed by Cu²⁺, which released more Li⁺ and facilitated faster migration. Consequently, the electrolyte achieved a high ionic conductivity of 0.2 mS cm⁻¹ and a transference number of 0.42 at 30 °C.

4.2. Mechanical Properties

The ion solvation structure in SPEs not only influences the ionic conductivity but also affects the mechanical properties of the electrolyte. There is generally a trade-off between the ionic conductivity and mechanical performance in conventional SPEs. Higher ionic conductivity typically requires the polymer matrix to have enhanced segmental mobility and lower structural density that impedes ion migration, which often correlates with greater polymer flexibility.^[70] However, excessive segmental mobility can reduce the mechanical strength of the polymer, making the electrolyte prone to deformation or fracture.^[71] Therefore, while improving ionic conductivity, it is crucial to ensure the polymer's crosslinking density and structural stability to maintain the electrolyte's mechanical integrity. Precisely tuning the Li⁺ solvation structure to optimize the balance between these factors is essential for achieving high-performance SPEs.

In SPEs, appropriately increasing the crosslinking density, such as by introducing intermolecular hydrogen bonding interactions,^[72] can balance ionic conductivity and mechanical performance. Xia et al.^[73] employed molecular engineering design strategies to develop an SPE with both high lithium-ion conductivity and excellent mechanical strength. As shown in Figure 6a, a copolymer of polyethylene glycol diacrylate (PEGDA) and 2-(3-(6-methyl-4-oxo-1,4-dihydropyrimidin-2-yl)ureido) ethyl methacrylate (UPyMA) was used to capture the deep eutectic electrolyte formed between N-methylurea (NML) and LiTFSI in a double-crosslinked network. The non-flammable, asymmetric bifunctional NML molecules participate in the solvation of Li⁺ via hydrogen bonding and ion-dipole interactions, promoting lithium salt dissociation and enhancing ionic conductivity. The soft PEGDA polymer functions as the amorphous region facilitating ion transport, while the dynamic hydrogen-bonded UPyMA dimers, characterized by their rigid, flat aromatic structures, assemble into fibrous networks in the condensed phase. This assembly reinforces the soft polymer matrix, mitigating deformation during the cycling process of the polymer electrolyte. Huang et al.^[74] developed an organic-inorganic crosslinked poly(ether-polyurethane)-type electrolyte with self-healing properties. The amino-modified Zr-porphyrin-based MOFs (ZrMOFs) and short-chain polyethylene glycol (PEG) were covalently crosslinked to form a molecular scaffold network, facilitating fast Li⁺ transport (Figure 6b). ZrMOFs serve as multi-site crosslinking reaction nodes and chain extenders, with the crosslinked SPE displaying a rich hydrogen bonding network (urea and urethane groups). This electrolyte exhibits high mechanical strength (76.5 MPa) and excellent tensile properties (about 2050%). Moreover, the abundant ether oxygen/carbonyl oxygen and Lewis acid sites significantly enhance

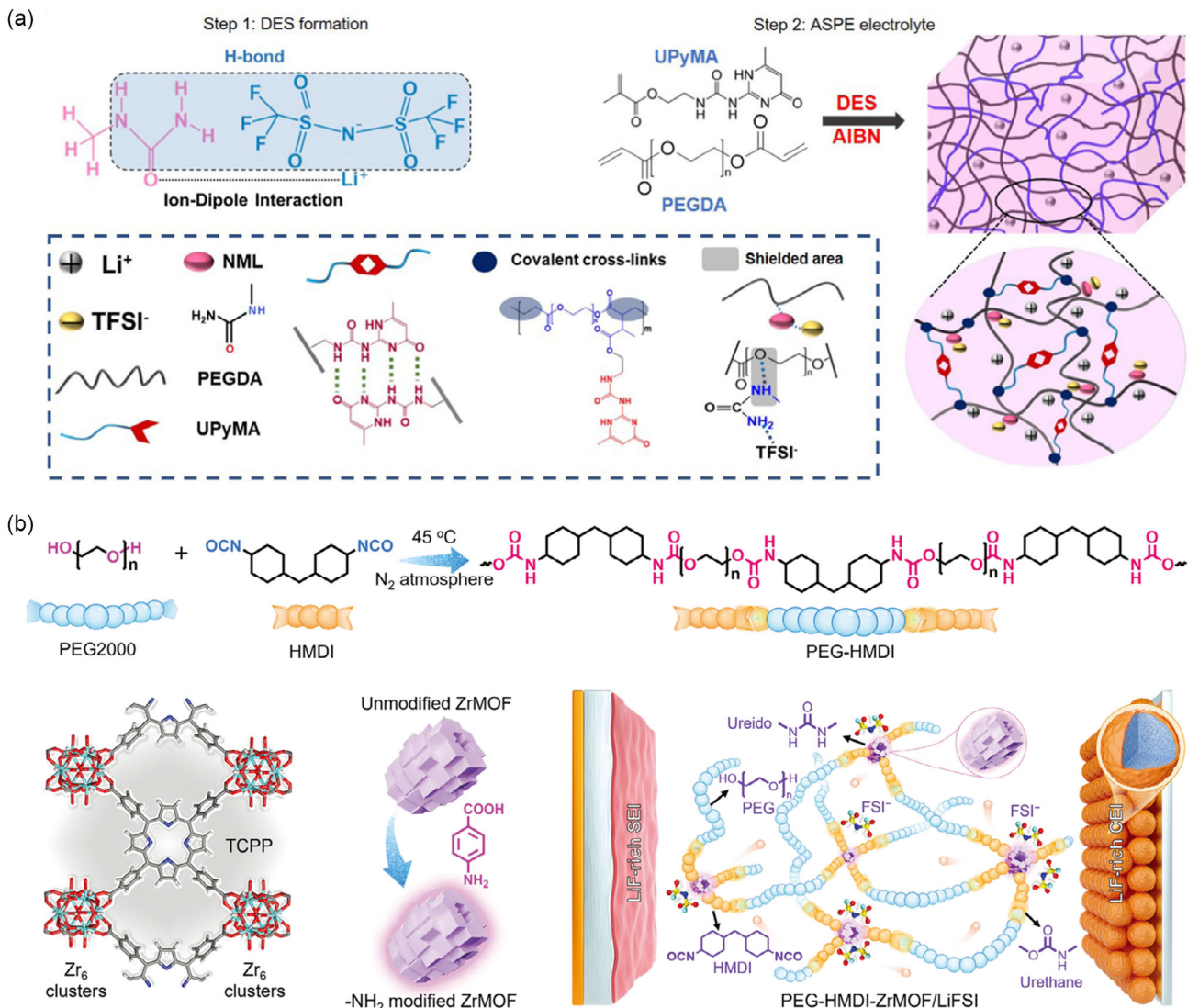


Figure 6. a) Illustrations for the synthesis process of multiple hydrogen bond crosslinked SPE (reprinted with permission.^[74] Copyright 2022, The Royal Society of Chemistry). b) Schematic for the preparation of ZrMOFs crosslinked SPE (reprinted with permission.^[75] Copyright 2024, Wiley-VCH GmbH).

the ionic conductivity of the SPE ($5.7 \times 10^{-4} \text{ S cm}^{-1}$ at 30°C) and Li^+ transference number (0.84).

Additionally, the use of polymer-induced phase separation (PIPS) technology is one of the effective strategies for decoupling the ionic conductivity and mechanical performance of SPEs.^[75] Bumjoon J. Kim and Seung Woo Lee et al. developed a series of elastic solid electrolytes with 3D interconnected plastic crystalline phases.^[76] These elastic electrolytes exhibit high mechanical strength, good ionic conductivity, and a high Li^+ transference number. In their study, the introduction of plastic crystalline phases (such as diene nitrile, SN) demonstrated high ionic conductivity when combined with lithium salts like LiTFSI. The plastic crystalline phases provide effective ionic transport channels, with their solvation structure enabling the rapid migration of lithium ions within the polymer matrix. By employing PIPS technology, the phase separation between the polymer matrix and the plastic crystalline phase is precisely controlled, resulting in the formation of a 3D interconnected

network structure (Figure 7a). The polymer matrix, based on elastomers like BA (Figure 7a),^[75] BA-co-ICA (Figure 7b),^[77] or TFEA (Figure 7c),^[78] acts as a solid diluent and has minimal impact on the solvation structure formed in the plastic crystalline phase. Therefore, this structure not only maintains the continuity of the polymer but also ensures that the ionic channels in the plastic crystalline phase are not disrupted, thus optimizing both ionic conductivity and mechanical properties.

Furthermore, plastic crystalline electrolytes based on SN have a wide electrochemical window, making them suitable for high-voltage solid-state lithium battery systems. However, the incompatible contact between Li metal and the electrolytes resulting from the side reaction of the Li metal-induced nitrile polymerization negatively affects the stability of the corresponding SN-based electrolytes,^[79] limiting their widespread application. Therefore, the chemical/electrochemical compatibility between such electrolytes and electrode materials still requires further investigation.

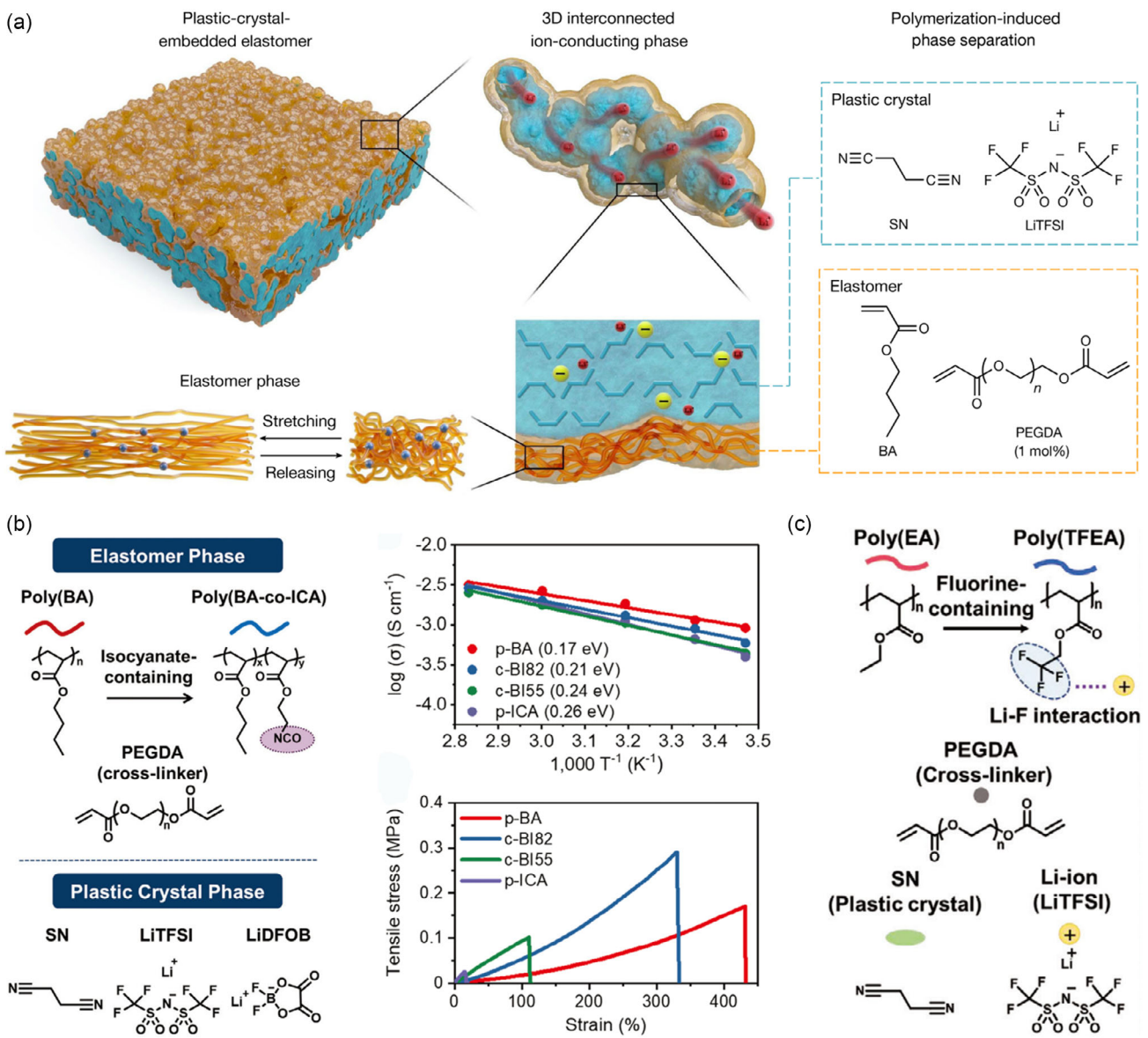


Figure 7. a) Design of plastic-crystal-embedded elastomer electrolyte (reprinted with permission.^[76] Copyright 2022, Springer Nature). b) Fabrication of iso-cyanate-incorporated phase-separated SPE, ion conductivity, and stress-strain curve analysis (reprinted with permission.^[78] Copyright 2024, Wiley-VCH GmbH). c) Fabrication of F-containing phase-separated SPE (reprinted with permission.^[79] Copyright 2024, Wiley-VCH GmbH).

4.3. Interfacial Stability

The interfacial stability between electrode materials and SPEs is a critical factor influencing the performance and lifespan of lithium batteries.^[80] When SPEs come into contact with lithium metal or high-voltage cathodes, complex electrochemical and chemical reactions can occur at the interface, leading to the formation of an unstable interfacial layer (SEI/CEI). This increases interfacial impedance and reduces the battery's performance.^[81] By fine-tuning the molecular design of the SPE and its corresponding solvation structure, it is possible to effectively improve the interfacial compatibility between the electrodes, suppress lithium dendrite growth, and enhance interfacial stability.

In recent years, electrolytes with weak solvation structures have garnered increasing attention. In weakly solvated electrolytes, both

solvent molecules (polymers) and anions coordinate with Li^+ , creating a solvation structure that is rich in anions under relatively dilute conditions.^[82] This alters the energy levels in the solvation structure, allowing anions to preferentially decompose on the electrode surface and form a stable, inorganic-rich interfacial layer that improves interfacial stability during cycling.

There are several methods to construct SPEs with weak solvation structures. For instance, Lewis acid additives^[83] can be introduced into the SPE, electron-withdrawing fluorine-containing segments/groups can be incorporated into the polymer structure,^[84] or bulky segments/groups with steric hindrance can be added.^[85] Wang et al.^[85a] introduced Lewis acids (Mg^{2+} and Al^{3+}) into the system, utilizing their strong electron-withdrawing ability to form coordination bonds with the strongly electronegative ether oxygen (EO) chains (Figure 8a).

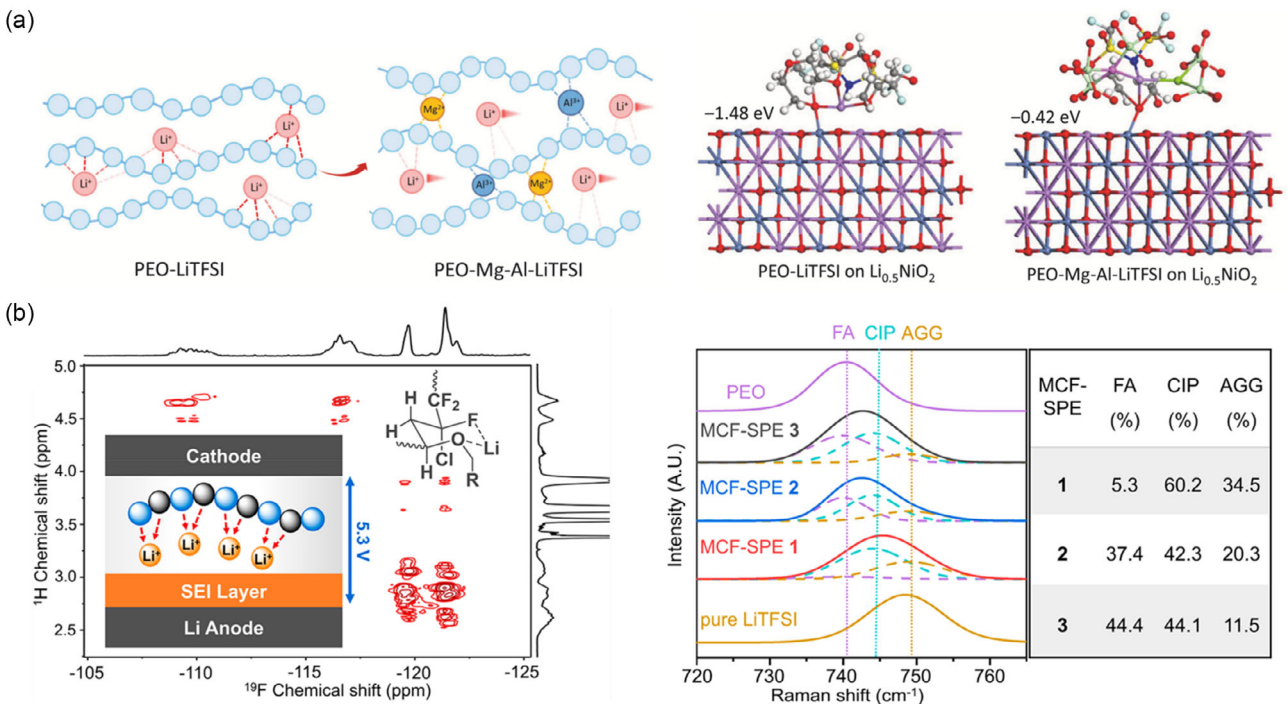


Figure 8. a) Schematic of the function of Lewis-acid additives and the adsorption energy of PEO-LiTFSI and PEO-Mg-Al-LiTFSI electrolytes on the half-lithiated Li_xNiO_2 (reprinted with permission.^[84a] Copyright 2024, The Authors). b) NMR and Raman characterization of weakly solvated fluorinated SPE (reprinted with permission.^[85a] Copyright 2021, American Chemical Society).

This interaction weakened the solvation ability of EO chains at high voltage, reducing the reactivity between EO chains and high-nickel cathodes. This effect significantly improved the interface compatibility of PEO-based polymer electrolytes with high-nickel cathodes at 4.8 V. Moreover, the typical coordination structures formed by Mg²⁺, Al³⁺, and other anions exhibited lower highest occupied molecular orbital (HOMO) energy levels, resulting in the formation of inorganic-rich interfacial layers. Consequently, PEO-based polymer electrolytes coordinated with Mg²⁺ and Al³⁺ exhibited excellent electrochemical stability (>5 V) and ionic conductivity (0.23 mS cm^{-1} at room temperature).

For the fluorine-containing SPEs, Chen et al.^[84a] synthesized a novel fluorine-containing polymer with a main chain of trifluorochloroethylene. Through 2D ¹H-¹⁹F NMR spectroscopy, they observed that the fluorine atoms in this polymer formed a stable 6-membered ring solvation structure with Li⁺, converting the strong Li⁺-O interaction into a weaker Li⁺-F interaction. This modification allowed more anions to enter the solvation structure, forming abundant CIP and tight ion pairs (Figure 8b). As a result, an anion-decomposition-dominated interfacial layer was formed, enhancing the redox stability of the polymer electrolyte. This material showed excellent stability with the lithium anode, with batteries in lithium plating-stripping tests exhibiting stable cycling for over 2600 h and effectively suppressing lithium dendrite formation. Additionally, the electrochemical window of the material was widened to 5.3 V, and lithium batteries assembled with LiCoO₂ or NCM811 cathodes using this material could stably cycle at a cutoff voltage of 4.5 V.

For the SPEs with steric hindrance, Zheng et al.^[85a] modified the solvent molecular structure of the precursor electrolyte by replacing the five-membered ring 1,3-dioxolane (DOL) with the

six-membered ring 1,3-dioxane (DOX) and initiated *in situ* ring-opening polymerization to form a polymer electrolyte using a Lewis acid. The resulting poly(DOX) polymer, with its extended alkyl chains, exhibited excellent oxidation stability (over 4.7 V) due to a lower HOMO energy level (Figure 9a). Additionally, the extended alkyl chains weakened the solvation ability, which not only provided a higher Li⁺ transference number (0.75) but also helped form a robust and inorganic-rich SEI layer. In addition, our group^[85] synthesized a polymer electrolyte (PDMA-Li) with a rich anion solvation structure by introducing various strengths of Li⁺-O interactions and sterically hindered groups into the polymer backbone. The repeating units of the synthesized polymer backbone contained one ether group, two ester groups, and a methyl group as a steric hindrance group. The ether oxygens can form strong ion-dipole interactions with Li⁺, increasing the polymer chain flexibility and promoting Li⁺ conduction along the chain. The ester group oxygens form weaker ion-dipole interactions with Li⁺, disrupting the tight coordination structure between ether oxygen and Li⁺, thereby enhancing Li⁺ migration. The methyl group, acting as a steric hindrance group, further inhibits the binding of Li⁺ to the polymer chain. Additionally, the C-H group on the methyl group, as a weak positive dipole, can form ion-dipole interactions with the anions, restricting their movement and further enhancing the Li⁺ transference number (Figure 9b). The resulting polymer electrolyte exhibited a high Li⁺ transference number of 0.8, a widened electrochemical window of 5.5 V, and the formation of a substantial number of tightly bound ion pairs. This facilitated the anion decomposition at the electrode surface, forming a highly electrochemically stable inorganic-rich interfacial layer. Lithium metal batteries assembled

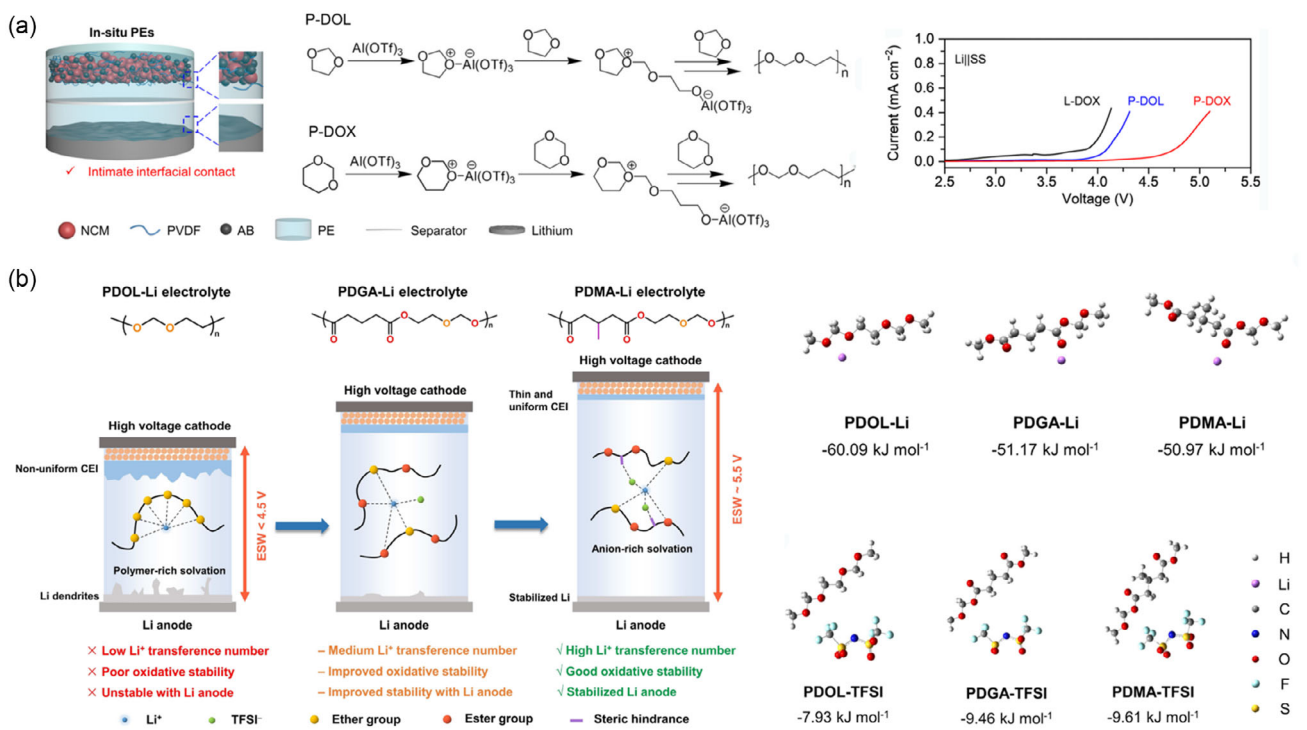


Figure 9. a) In situ polymerization of DOL and DOX in the battery, and the comparison of linear sweep voltammetry with different electrolytes (reprinted with permission.^[86a] Copyright 2023, The Royal Society of Chemistry). b) Schematic illustration of the electrolytes with different steric structures and binding energy analysis (reprinted with permission.^[86b] Copyright 2024, Wiley-VCH GmbH).

with this electrolyte demonstrated stable cycling at cutoff voltages of 4.5 V.

5. Summary and Outlook

In this review, we try to provide a perspective of solvation structure to understand the performance of SPEs in lithium-based batteries, focusing on their ionic conductivity, mechanical properties, and interfacial stability. We first outline the key characteristics and driving forces of the solvation structure for the SPEs. Then, we describe the techniques including spectral analysis and theoretical simulation to characterize solvation structures in SPEs. Finally, we explore the relationship between solvation structure and electrochemical performance, discussing strategies to enhance battery performance through solvation structure optimization.

The modulation of solvation behavior in SPEs has emerged as a critical avenue for enhancing the performance of lithium-based batteries. The interaction of electrolyte components, even at small scales, can significantly alter the electrochemical behavior of the battery. However, the development of solvation theory and its application to SPEs still face several longstanding challenges. First, we lack sufficient characterization techniques capable of directly probing the solvation behavior in solid-state lithium batteries. Traditional techniques such as NMR, Raman, and FTIR spectroscopy can only provide information about the bulk phase of the electrolyte, but they are unable to accurately describe important features such as the local solvation environment and ion arrangement at the interface. This is especially challenging in

SPEs, where the solvation structure typically exhibits highly localized and dynamic characteristics, and the characterization of these localized behaviors remains a pressing issue. Then, simplistic theoretical models overly. Current theoretical models for solvation structures often focus on simplified interactions, typically considering only the most dominant forces, such as ion–dipole or electrostatic interactions. However, many other intermolecular forces, such as van der Waals forces and even more complex induced interactions, are often neglected. This oversimplification severely limits the accuracy of existing solvation models and their ability to predict SPEs performance under different operating conditions. Finally, the scalability of solid-state battery technology and its commercialization potential remain key obstacles, and more research is needed to overcome these challenges. To address the above challenges, some potentially promising solutions are provided.

1) Multiscale characterization techniques. Given the dynamic nature of solvation and desolvation processes, a multiscale approach combining time- and space-resolved techniques is essential to unravel the complexities of solvation behavior in SPEs. The application of ultrafast electron diffraction and time-resolved X-ray diffraction technologies, which have yet to be fully exploited in battery research, holds significant potential for capturing the transient solvation and desolvation events. These methods would allow real-time observation of solvation dynamics at both the molecular and interface levels, providing critical insights into the evolution of solvation structures during battery operation. Such advanced techniques, especially in situ characterization, will provide a comprehensive understanding of solvation

structures across both time and spatial dimensions, offering new perspectives on solvation structure in SPEs.

2) Integration of bulk solvation structures and electrode–electrolyte interphase (CEI/SEI) theories. Solvation theory and CEI/SEI theory are complementary frameworks that collectively bridge the gap between the molecular-level dynamics and macroscopic electrochemical performance of batteries. There is consensus that electrochemical reactions occur at the Helmholtz layer,^[86] where the solvation structure of SPEs would change during the charging/discharging process. And the interface solvation structure is highly correlated with the anodic/cathodic stability of SPEs. Current theoretical simulations of the bulk solvation structure, while insightful, do not universally capture all experimental observations on the enhanced performance of the electrolyte. To address these limitations, we propose the integration of multiscale simulation techniques combining atomic details with mesoscale behavior to further refine the solvation structure theory; incorporate explicit ion–polymer and ion–interface interactions, and perform systematic validation of the stability of CEIs and SEIs through *in situ* experimental studies. By integrating these two theories, researchers can develop more comprehensive models that consider both the bulk electrolyte properties and the interface dynamics. Such integrated models will provide better predictive capabilities for designing SPEs that not only exhibit high ionic conductivity but also form stable and robust interphases with electrodes, ultimately enhancing battery efficiency and cycle life.

3) Machine learning and artificial intelligence (AI) for solvation optimization. The application of cutting-edge computational techniques, such as machine learning and AI, is poised to revolutionize the design of solvation structures in SPEs. Machine learning algorithms can be employed to simulate the behavior of thousands of molecules in complex electrolyte environments, identifying trends, patterns, and key interactions that govern solvation dynamics. This approach enables the systematic exploration of vast compositional spaces to identify optimal combinations of polymer matrix, anions, and additives that can enhance solvation properties and improve electrolyte performance. Furthermore, AI-based systems can be integrated with experimental data to predict the solvation behavior of new materials, providing a powerful tool for designing next-generation SPEs with tailored properties.

Future research should focus on overcoming the trade-offs inherent in solvation design, developing novel SPE chemistries, and bridging the gap between laboratory research and industrial applications. With continued innovation and collaboration, the next generation of SPEs will play a key role in the commercialization of high-performance lithium-based batteries for a wide range of applications.

Acknowledgements

T.C. and Y.L. contributed equally to this work. This work is financially supported by the National Natural Science Foundation of China (grant nos. 22425504 and 22405220), the Sichuan Science and Technology Program (grant no. 2024NSFSC1155),

and the Chengdu Guojia Electrical Engineering Co., Ltd. (no. NEEC-2022-B20).

Conflict of Interest

The authors declare no conflict of interest.

Keywords: intermolecular interactions · lithium-based batteries · solid polymer electrolyte · solvation structure

- [1] a) X. Lu, Y. M. Wang, X. Y. Xu, B. G. Yan, T. Wu, L. Lu, *Adv. Energy Mater.* **2023**, *13*, 2301746; b) J. Janek, W. G. Zeier, *Nat. Energy* **2023**, *8*, 230; c) Q. Zhao, S. Stalin, C. Z. Zhao, L. A. Archer, *Nat. Rev. Mater.* **2020**, *5*, 229.
- [2] a) S. H. Zhang, F. Sun, X. F. Du, X. H. Zhang, L. Huang, J. Ma, S. M. Dong, A. Hilger, I. Manke, L. S. Li, B. Xie, J. D. Li, Z. W. Hu, A. C. Komarek, H. J. Lin, C. Y. Kuo, C. T. Chen, P. X. Han, G. J. Xu, Z. L. Cui, G. L. Cui, *Energy Environ. Sci.* **2023**, *16*, 2591; b) Y. X. Ma, J. Y. Wan, Y. F. Yang, Y. S. Ye, X. Xiao, D. T. Boyle, W. Burke, Z. J. Huang, H. Chen, Y. Cui, Z. A. Yu, S. T. Oyakhire, *Adv. Energy Mater.* **2022**, *12*, 2103720; c) L. S. Zhang, P. P. Zhang, C. Y. Chang, W. B. Guo, Z. H. Guo, X. Pu, *ACS Appl. Mater. Int.* **2021**, *13*, 46794.
- [3] a) M. L. Nguyen, V.-C. Nguyen, Y.-L. Lee, J.-S. Jan, H. Teng, *Energy Storage Mater.* **2024**, *65*, 103178; b) C. Z. Zhao, Q. Zhao, X. Liu, J. Zheng, S. Stalin, Q. Zhang, L. A. Archer, *Adv. Mater.* **2020**, *32*, e1905629.
- [4] a) M. H. Chen, Z. Y. Yue, Y. X. Wu, Y. Wang, Y. Li, Z. Chen, *Sustainable Mater. Technol.* **2023**, *36*, e00587; b) E. K. W. Andersson, C. Sångeland, E. Berggren, F. O. L. Johansson, D. Kühn, A. Lindblad, J. Mindemark, M. Hahlén, *J. Mater. Chem. A* **2021**, *9*, 22462.
- [5] a) Y. Gong, C. Wang, M. Xin, S. Chen, P. Xu, D. Li, J. Liu, Y. Wang, H. Xie, X. Sun, Y. Liu, *Nano Energy* **2024**, *119*, 109054; b) S. Usta, M. Çelik, T. Çetinkaya, *J. Power Sources* **2023**, *580*, 233404; c) X. Yang, M. Jiang, X. Gao, D. Bao, Q. Sun, N. Holmes, H. Duan, S. Mukherjee, K. Adair, C. Zhao, J. Liang, W. Li, J. Li, Y. Liu, H. Huang, L. Zhang, S. Lu, Q. Lu, R. Li, C. V. Singh, X. Sun, *Energy Environ. Sci.* **2020**, *13*, 1318.
- [6] a) L. Bertoli, G. Gabriele, E. Gibertini, L. Magagnin, *J. Energy Storage* **2024**, *81*, 110456; b) S. S. Qian, H. Chen, Z. Z. Wu, D. S. Li, X. H. Liu, Y. B. Tang, S. Q. Zhang, *Batteries Supercaps* **2021**, *4*, 39; c) Y. Mallaiyah, V. R. Jeedi, R. Swarnalatha, A. Raju, S. Narendra Reddy, A. Sadananda Chary, *J. Phys. Chem. Solids* **2021**, *155*, 110096.
- [7] a) B. Y. Huang, P. B. Lai, H. M. Hua, R. Y. Li, X. Shen, X. Y. Yang, P. Zhang, J. B. Zhao, *J. Power Sources* **2023**, *570*, 233049; b) Y. B. He, N. Liu, P. A. Kohl, *J. Power Sources* **2021**, *481*, 228832; c) A. Bergfelt, G. Hernández, R. Mogensen, M. J. Lacey, J. Mindemark, D. Brandell, T. M. Bowden, *ACS Appl. Polym. Mater.* **2020**, *2*, 939.
- [8] a) N. Xu, Y. Zhao, M. H. Ni, J. Zhu, X. C. Song, X. Q. Bi, J. P. Zhang, H. T. Zhang, Y. F. Ma, C. X. Li, Y. S. Chen, *Angew. Chem. Int. Ed.* **2024**, *63*, e202404400; b) K. X. Mu, D. Wang, W. L. Dong, Q. Liu, Z. N. Song, W. J. Xu, P. P. Yao, Y. A. Chen, B. Yang, C. H. Li, L. Tian, C. Z. Zhu, J. Xu, *Adv. Mater.* **2023**, *35*, 2304686; c) S. J. Wen, C. Luo, Q. R. Wang, Z. Y. Wei, Y. X. Zeng, Y. D. Jiang, G. Z. Zhang, H. L. Xu, J. Wang, C. Y. Wang, J. Chang, Y. H. Deng, *Energy Storage Mater.* **2022**, *47*, 453.
- [9] a) K. H. Tang, Q. S. Bai, P. W. Xu, R. L. Liu, S. F. Xue, S. H. Liu, Y. L. Zhu, *Small Methods* **2024**, *8*, 2301810; b) S. M. Hao, S. Liang, C. D. Sewell, Z. L. Li, C. Z. Zhu, J. Xu, Z. Q. Lin, *Nano Lett.* **2021**, *21*, 7435; c) H. C. Wang, Q. Wang, X. Cao, Y. Y. He, K. Wu, J. J. Yang, H. H. Zhou, W. Liu, X. M. Sun, *Adv. Mater.* **2020**, *32*, 2001259.
- [10] a) G. J. Zeng, S. Q. Dai, X. P. Chen, L. Qiu, X. Kong, M. J. Huang, T. Wen, *Macromolecules* **2024**, *57*, 1258; b) H. L. Liu, L. Mulderig, D. Hallinan, H. Y. Chung, *Macromol. Rapid Commun.* **2021**, *42*, 2000428; c) K. Guo, S. Li, G. Chen, J. Wang, Y. Wang, X. Xie, Z. Xue, *CCS Chem.* **2022**, *4*, 3134.
- [11] a) P. F. Zhai, N. Ahmad, S. Q. Qu, L. G. Feng, W. Yang, *Adv. Funct. Mater.* **2024**, *34*, 2316561; b) M. C. Nguyen, H. L. Nguyen, T. P. M. Duong, S. H. Kim, J. Y. Kim, J. H. Bae, H. K. Kim, S. N. Lim, W. Ahn, *Adv. Funct. Mater.* **2024**, *34*, 2406987; c) Y. H. Li, Y. Y. Qin, J. Y. Zhao, M. B. Ma, M. Z. Zhang, P. Li, S. Y. Lu, H. T. Bu, K. Xi, Y. Q. Su, S. J. Ding, *ACS Appl. Mater. Inter.* **2022**, *14*, 18360.
- [12] X. Chen, Q. Zhang, *Acc. Chem. Res.* **2020**, *53*, 1992.
- [13] Z. Song, M. Tian, J. Zhu, J. Chen, W. Feng, L. Ben, H. Yu, X. Huang, M. Armand, Z. Zhou, H. Zhang, *Adv. Mater.* **2024**, *36*, 2410954.

- [14] a) C. Wang, H. Liu, Y. Liang, D. Li, X. Zhao, J. Chen, W. Huang, L. Gao, L. Z. Fan, *Adv. Funct. Mater.* **2022**, *33*, 2209828; b) Y. Su, X. H. Rong, H. Li, X. J. Huang, L. Q. Chen, B. Y. Liu, Y.-S. Hu, *Adv. Mater.* **2023**, *35*, 2209402.
- [15] H. Xie, H. Liang, P. Kumar, H. Cheng, F. Zhao, Y. Wang, T. Cai, W. Wahyudi, Z. Ma, Q. Li, J. Ming, *Adv. Funct. Mater.* **2024**, *34*, 2401118.
- [16] Z. Piao, R. Gao, Y. Liu, G. Zhou, H. M. Cheng, *Adv. Mater.* **2022**, *35*, 2206009.
- [17] T. Hou, K. D. Fong, J. Wang, K. A. Persson, *Chem. Sci.* **2021**, *12*, 14740.
- [18] a) Q. Zhao, X. Liu, S. Stalin, K. Khan, L. A. Archer, *Nat. Energy* **2019**, *4*, 365; b) K. Guo, J. Wang, Z. Shi, Y. Wang, X. Xie, Z. Xue, *Angew. Chem. Int. Ed.* **2023**, *62*, e202213606.
- [19] H. Cheng, Q. Sun, L. Li, Y. Zou, Y. Wang, T. Cai, F. Zhao, G. Liu, Z. Ma, W. Wahyudi, Q. Li, J. Ming, *ACS Energy Lett.* **2022**, *7*, 490.
- [20] Z. Piao, P. Xiao, R. Luo, J. Ma, R. Gao, C. Li, J. Tan, K. Yu, G. Zhou, H. M. Cheng, *Adv. Mater.* **2022**, *34*, 2108400.
- [21] R. Li, H. Hua, X. Yang, J. Tian, Q. Chen, R. Huang, X. Li, P. Zhang, J. Zhao, *Energy Environ. Sci.* **2024**, *17*, 5601.
- [22] a) Y. F. Huang, T. Gu, G. C. Rui, P. R. Shi, W. B. Fu, L. Chen, X. T. Liu, J. P. Zeng, B. H. Kang, Z. C. Yan, F. J. Stadler, L. Zhu, F. Y. Kang, Y. B. He, *Energy Environ. Sci.* **2021**, *14*, 6021; b) L. Zhu, *J. Phys. Chem. Lett.* **2014**, *5*, 3677.
- [23] Z. M. Zhao, F. Li, J. W. Zhao, G. L. Ding, J. Z. Wang, X. F. Du, Q. Zhou, G. J. Hou, G. L. Cui, *Adv. Funct. Mater.* **2020**, *30*, 2000347.
- [24] Y. Aihara, K. Sugimoto, W. S. Price, K. Hayamizu, *J. Chem. Phys.* **2000**, *113*, 1981.
- [25] K. Xu, *Chem. Rev.* **2004**, *104*, 4303.
- [26] D. J. Siegel, L. Nazar, Y.-M. Chiang, C. Fang, N. P. Balsara, *Trends Chem.* **2021**, *3*, 807.
- [27] a) V. Bocharova, A. P. Sokolov, *Macromolecules* **2020**, *53*, 4141; b) Z. Li, J. Fu, X. Zhou, S. Gui, L. Wei, H. Yang, H. Li, X. Guo, *Adv. Sci.* **2023**, *10*, 2201718.
- [28] H. Wang, L. Sheng, G. Yasin, L. Wang, H. Xu, X. He, *Energy Storage Mater.* **2020**, *33*, 188.
- [29] D. Lu, R. Li, M. M. Rahman, P. Yu, L. Lv, S. Yang, Y. Huang, C. Sun, S. Zhang, H. Zhang, J. Zhang, X. Xiao, T. Deng, L. Fan, L. Chen, J. Wang, E. Hu, C. Wang, X. Fan, *Nature* **2024**, *627*, 101.
- [30] H. Jiang, Q. Zhang, Y. Zhang, L. Sui, G. Wu, K. Yuan, X. Yang, *Phys. Chem. Chem. Phys.* **2019**, *21*, 10417.
- [31] C. Y. Son, Z. G. Wang, *J. Chem. Phys.* **2020**, *153*, 100903.
- [32] a) M. A. Ratner, P. Johansson, D. F. Shriver, *MRS Bull.* **2000**, *25*, 31; b) D. Bresser, S. Lyonnard, C. Iojoiu, L. Picard, S. Passerini, *Mol. Syst. Des. Eng.* **2019**, *4*, 779; c) G. S. MacGlashan, Y. G. Andreev, P. G. Bruce, *Nature* **1999**, *398*, 792.
- [33] P. Lightfoot, M. A. Mehta, P. G. Bruce, *Science* **1993**, *262*, 883.
- [34] Z. Song, F. Chen, M. Martinez-Ibañez, W. Feng, M. Forsyth, Z. Zhou, M. Armand, H. Zhang, *Nat. Commun.* **2023**, *14*, 4884.
- [35] K. S. Lee, Z. Landry, F. C. Pereira, M. Wagner, D. Berry, W. E. Huang, G. T. Taylor, J. Kneipp, J. Popp, M. Zhang, J.-X. Cheng, R. Stocker, *Nat. Rev. Methods Primers* **2021**, *1*, 80.
- [36] a) I. Rey, J. C. Lassègues, J. Grondin, L. Servant, *Electrochim. Acta* **1998**, *43*, 1505; b) J. Nanda, G. Yang, T. Hou, D. N. Voylov, X. Li, R. E. Ruther, M. Naguib, K. Persson, G. M. Veith, A. P. Sokolov, *Joule* **2019**, *3*, 2001; c) B. Huang, Z. Wang, G. Li, H. Huang, R. Xue, L. Chen, F. Wang, *Solid State Ion* **1996**, *85*, 79.
- [37] L. Edman, *J. Phys. Chem. B* **2000**, *104*, 7254.
- [38] K. Kimura, J. Motomatsu, Y. Tominaga, *J. Phys. Chem. C* **2016**, *120*, 12385.
- [39] B. Reif, S. E. Ashbrook, L. Emsley, M. Hong, *Nat. Rev. Methods Primers* **2021**, *1*, 2.
- [40] a) L. Y. Yang, D. X. Wei, M. Xu, Y. F. Yao, Q. Chen, *Angew. Chem. Int. Ed.* **2014**, *53*, 3631; b) J. Li, Z. Hu, S. Zhang, H. Zhang, S. Guo, G. Zhong, Y. Qiao, Z. Peng, Y. Li, S. Chen, G. Chen, A.-M. Cao, *Nat. Sustainable* **2024**, *7*, 1481; c) Y. Wang, C. J. Zanelotti, X. Wang, R. Kerr, L. Jin, W. H. Kan, T. J. Dingemans, M. Forsyth, L. A. Madsen, *Nat. Mater.* **2021**, *20*, 1255.
- [41] S. T. Han, P. Wen, H. J. Wang, Y. Zhou, Y. Gu, L. Zhang, Y. Shao-Horn, X. Lin, M. Chen, *Nat. Mater.* **2023**, *22*, 1515.
- [42] X. Liu, L. Fang, X. Lyu, R. E. Winans, T. Li, *Chem. Mater.* **2023**, *35*, 9821.
- [43] C. M. Jeffries, J. Ilavsky, A. Martel, S. Hinrichs, A. Meyer, J. S. Pedersen, A. V. Sokolova, D. I. Svergun, *Nat. Rev. Methods Primers* **2021**, *1*, 70.
- [44] S. Inceoglu, A. A. Rojas, D. Devaux, X. C. Chen, G. M. Stone, N. P. Balsara, *ACS Macro Lett.* **2014**, *3*, 510.
- [45] S. Wang, H. Shi, D. Wang, Y. Xia, Y. Yin, S. Liang, Y. Hu, R. Shao, X. Wu, Z. Xu, *Nano Energy* **2024**, *122*, 109337.
- [46] W. S. Loo, K. I. Mongcopia, D. A. Gribble, A. A. Faraone, N. P. Balsara, *Macromolecules* **2019**, *52*, 8724.
- [47] M. Kruteva, *Adsorption* **2021**, *27*, 875.
- [48] G. Mao, R. F. Perea, W. S. Howells, D. L. Price, M.-L. Saboungi, *Nature* **2000**, *405*, 163.
- [49] N. J. Shah, C. Fang, N. C. Osti, E. Mamontov, X. Yu, J. Lee, H. Watanabe, R. Wang, N. P. Balsara, *Nat. Mater.* **2024**, *23*, 664.
- [50] W. F. van Gunsteren, H. J. C. Berendsen, *Angew. Chem. Int. Ed.* **2003**, *42*, 992.
- [51] a) O. Borodin, G. D. Smith, *Macromolecules* **2006**, *39*, 1620; b) N. Molinari, J. P. Mailoa, B. Kozinsky, *Chem. Mater.* **2018**, *30*, 6298; c) F. Müller-Plathe, W. F. van Gunsteren, *J. Chem. Phys.* **1995**, *103*, 4745; d) T. Xie, A. France-Lanord, Y. Wang, J. Lopez, M. A. Stolberg, M. Hill, G. M. Leverick, R. Gomez-Bombarelli, J. A. Johnson, Y. Shao-Horn, J. C. Grossman, *Nat. Commun.* **2022**, *13*, 3415.
- [52] K. S. Pitzer, *J. Phys. Chem.* **1973**, *77*, 268.
- [53] M. A. Webb, Y. Jung, D. M. Pesko, B. M. Savoie, U. Yamamoto, G. W. Coates, N. P. Balsara, Z. G. Wang, T. F. Miller III, *ACS Cent. Sci.* **2015**, *1*, 198.
- [54] D. G. Mackanic, W. Michaels, M. Lee, D. Feng, J. Lopez, J. Qin, Y. Cui, Z. Bao, *Adv. Energy Mater.* **2018**, *8*, 1800703.
- [55] Z. Yang, J. Cai, Z. Shen, J. Bian, J. Chen, Y. Xu, Z. Fang, C. Du, X. Xiang, J. Wang, P. Yu, R. Cui, S. Bi, *Macromolecules* **2024**, *57*, 4460.
- [56] a) S. Li, L. Li, H. Yang, Y. Zhao, Y. Shan, *Chem. Eng. J.* **2024**, *484*, 149433; b) X. Y. Zhang, M. V. M. Nitou, W. J. Li, Z. Wan, L. F. Liu, Z. H. Luo, S. Muhammad, W. Qin, L. An, Y. H. Niu, W. Q. Lv, *Chin. Chem. Lett.* **2023**, *34*, 108245; c) D. M. Reinoso, M. A. Frecher, *Energy Storage Mater.* **2022**, *52*, 430.
- [57] C. Fang, S. Chakraborty, Y. Li, J. Lee, N. P. Balsara, R. Wang, *ACS Macro Lett.* **2023**, *12*, 1244.
- [58] a) X. Y. Shan, Z. W. Song, H. Ding, L. W. Li, Y. H. Tian, A. P. Sokolov, M. Tian, K. Xu, P. F. Cao, *Energy Environ. Sci.* **2024**, *17*, 8457; b) H. Gudla, C. Zhang, D. Brandell, *J. Phys. Chem. B* **2020**, *124*, 8124; c) Q. Zhou, J. Ma, S. Dong, X. Li, G. Cui, *Adv. Mater.* **2019**, *31*, e1902029.
- [59] C. Deng, P. Bennington, R. J. Sánchez-Leija, S. N. Patel, P. F. Nealey, J. de Pablo, *Macromolecules* **2023**, *56*, 8069.
- [60] S. Han, P. Wen, H. Wang, Y. Zhou, Y. Gu, L. Zhang, Y. Shao-Horn, X. Lin, M. Chen, *Nat. Mater.* **2023**, *22*, 1515.
- [61] Y. Liu, Q. Zeng, Z. Li, A. Chen, J. Guan, H. Wang, S. Wang, L. Zhang, *Adv. Sci.* **2023**, *10*, e2206978.
- [62] J. Wang, S. Li, Q. Zhao, C. Song, Z. Xue, *Adv. Funct. Mater.* **2020**, *31*, 2008208.
- [63] E. T. Röchow, M. Coeler, D. Pospiech, O. Kobsch, E. Mechtaeva, R. Vogel, B. Voit, K. Nikoliczki, M. Wolter, *Polymers* **2020**, *12*, 1707.
- [64] K. Zhang, F. Wu, X. Wang, L. Zheng, X. Yang, H. Zhao, Y. Sun, W. Zhao, Y. Bai, C. Wu, *Adv. Funct. Mater.* **2021**, *32*, 2107764.
- [65] a) T. Dong, H. Zhang, R. Hu, P. Mu, Z. Liu, X. Du, C. Lu, G. Lu, W. Liu, G. Cui, *Energy Storage Mater.* **2022**, *50*, 525; b) C. Wang, H. Zhang, S. Dong, Z. Hu, R. Hu, Z. Guo, T. Wang, G. Cui, L. Chen, *Chem. Mater.* **2020**, *32*, 9167.
- [66] a) F. Q. Li, B. Xu, X. B. Geng, S. Q. Guo, S. Wang, D. G. Li, *Ionics* **2024**, *30*, 145; b) M. Martinez-Ibañez, N. Boaretto, L. Meabe, X. E. Wang, H. J. Zhu, A. Santiago, O. Zugazua, M. Forsyth, M. Armand, H. Zhang, *Chem. Mater.* **2022**, *34*, 7493; c) Y. Tominaga, K. Yamazaki, V. Nanthana, *J. Electrochem. Soc.* **2015**, *162*, A3133; d) H. Z. Jiang, X. Q. Han, X. F. Du, Z. Chen, C. L. Lu, X. T. Li, H. R. Zhang, J. W. Zhao, P. X. Han, G. L. Cui, *Adv. Mater.* **2022**, *34*, 2108665.
- [67] H. Chen, M. T. Zheng, S. S. Qian, H. Y. Ling, Z. Z. Wu, X. H. Liu, C. Yan, S. Q. Zhang, *Carbon Energy* **2021**, *3*, 929.
- [68] H. Y. Zhou, Y. Ou, S. S. Yan, J. Xie, P. Zhou, L. Wan, Z. A. Xu, F. X. Liu, W. L. Zhang, Y. C. Xia, K. Liu, *Angew. Chem. Int. Ed.* **2023**, *62*, e202306948.
- [69] Y. Wei, T. H. Liu, W. Zhou, H. Cheng, X. Liu, J. Kong, Y. Shen, H. Xu, Y. Huang, *Adv. Energy Mater.* **2023**, *13*, 2203547.
- [70] a) J. Hu, W. H. Wang, Y. Zhou, B. B. Dong, S. H. He, J. G. Sun, H. Yan, Y. Z. Feng, L. Lu, *J. Energy Storage* **2024**, *103*, 114391; b) G. L. Lu, Y. J. Zhang, J. J. Zhang, X. F. Du, Z. L. Lv, J. Z. Du, Z. M. Zhao, Y. Tang, J. W. Zhao, G. L. Cui, *Carbon Energy* **2023**, *5*, e287.
- [71] a) X. Tong, Z. Tian, J. Sun, V. Tung, R. B. Kaner, Y. Shao, *Mater. Today* **2021**, *44*, 78; b) K. S. Ngai, S. Ramesh, K. Ramesh, J. C. Juan, *Ionics* **2016**, *22*, 1259.
- [72] a) Y. An, X. Han, Y. Y. Liu, A. Azhar, J. Na, A. K. Nanjundan, S. P. Wang, J. X. Yu, Y. Yamauchi, *Small* **2022**, *18*, 2103617; b) N. Meng, F. Lian, G. L. Cui, *Small* **2021**, *17*, 2005762.
- [73] H. Wang, J. Song, K. Zhang, Q. Fang, Y. Zuo, T. Yang, Y. Yang, C. Gao, X. Wang, Q. Pang, D. Xia, *Energy Environ. Sci.* **2022**, *15*, 5149.
- [74] F. Pei, Y. M. Huang, L. Wu, S. Y. Zhou, Q. Kang, W. J. Lin, Y. Q. Liao, Y. Zhang, K. Huang, Y. Shen, L. X. Yuan, S. G. Sun, Z. Li, Y. H. Huang, *Adv. Mater.* **2024**, *36*, 2409629.
- [75] M. J. Lee, J. Han, K. Lee, Y. J. Lee, B. G. Kim, K. N. Jung, B. J. Kim, S. W. Lee, *Nature* **2022**, *601*, 217.

- [76] a) S. H. Kwon, M. J. Lee, J. Han, J. H. Min, S. Kim, S. Y. Kim, J. Park, E. Lee, S. W. Lee, B. J. Kim, *J. Mater. Chem. A* **2024**, *12*, 3460; b) J. Han, M. J. Lee, K. Lee, Y. J. Lee, S. H. Kwon, J. H. Min, E. Lee, W. Lee, S. W. Lee, B. J. Kim, *Adv. Mater.* **2022**, *35*, 2205194.
- [77] S. Kim, M. J. Lee, S. H. Kwon, J. Park, Y. Byun, J. Choi, H. Seong, H. S. Kwon, E. Lee, S. W. Lee, B. J. Kim, *Adv. Energy Mater.* **2024**, *14*, 2403846.
- [78] J. Han, M. J. Lee, J. H. Min, K. H. Kim, K. Lee, S. H. Kwon, J. Park, K. Ryu, H. Seong, H. Kang, E. Lee, S. W. Lee, B. J. Kim, *Adv. Funct. Mater.* **2024**, *34*, 2310801.
- [79] D. Bao, W. Zhao, Z. Li, Y. Tao, Y. Zhong, Z. Tang, Z. Gao, H. Wang, H. Zhang, X. Sun, *J. Energy Storage* **2024**, *91*, 112016.
- [80] J. Pan, P. Zhao, N. N. Wang, F. Q. Huang, S. X. Dou, *Energy Environ. Sci.* **2022**, *15*, 2753.
- [81] a) Z. Y. Wang, C. Z. Zhao, S. Sun, Y. K. Liu, Z. X. Wang, S. Li, R. Zhang, H. Yuan, J. Q. Huang, *Matter-Us* **2023**, *6*, 1096; b) P. P. Ding, Z. Y. Lin, X. W. Guo, L. Q. Wu, Y. T. Wang, H. X. Guo, L. L. Li, H. J. Yu, *Mater. Today* **2021**, *51*, 449.
- [82] a) P. Xu, Y. C. Gao, Y. X. Huang, Z. Y. Shuang, W. J. Kong, X. Y. Huang, W. Z. Huang, N. Yao, X. Chen, H. Yuan, C. Z. Zhao, J. Q. Huang, Q. Zhang, *Adv. Mater.* **2024**, *36*, 2409489; b) C. Wang, X. Zhao, D. Li, C. Yan, Q. Zhang, L. Z. Fan, *Angew. Chem. Int. Ed.* **2024**, *136*, e202317856.
- [83] a) H. An, M. Li, Q. Liu, Y. Song, J. Liu, Z. Yu, X. Liu, B. Deng, J. Wang, *Nat. Commun.* **2024**, *15*, 9150; b) C. Zhang, S. Zhang, Y. Zhang, X. Wu, L. Lin, X. Hu, L. Wang, J. Lin, B. Sa, G. Wei, D.-L. Peng, Q. Xie, *Small Struct.* **2023**, *5*, 2300301.
- [84] a) M. Ma, F. Shao, P. Wen, K. Chen, J. Li, Y. Zhou, Y. Liu, M. Jia, M. Chen, X. Lin, *ACS Energy Lett.* **2021**, *6*, 4255; b) M. Y. Jia, P. Wen, Z. T. Wang, Y. C. Zhao, Y. M. Liu, J. Lin, M. Chen, X. R. Lin, *Adv. Funct. Mater.* **2021**, *31*, 2101736.
- [85] a) Y. Liu, H. Zou, Z. Huang, Q. Wen, J. Lai, Y. Zhang, J. Li, K. Ding, J. Wang, Y.-Q. Lan, Q. Zheng, *Energy Environ. Sci.* **2023**, *16*, 6110; b) Y. Liu, Z. Jin, Z. Liu, H. Xu, F. Sun, X. Q. Zhang, T. Chen, C. Wang, *Angew. Chem. Int. Ed.* **2024**, *63*, e202405802.
- [86] a) J. Luo, L. Xu, Y. Zhou, T. Yan, Y. Shao, D. Yang, L. Zhang, Z. Xia, T. Wang, L. Zhang, T. Cheng, Y. Shao, *Angew. Chem. Int. Ed.* **2023**, *62*, e202302302; b) X. Han, H. Jiang, P. Mu, W. Zhang, H. Zhang, G. Xu, Z. Chen, P. Han, G. Cui, *Angew. Chem. Int. Ed.* **2025**, *64*, e202412753.

Manuscript received: January 4, 2025

Revised manuscript received: March 12, 2025

Version of record online: March 15, 2025